Combined Optical and Radio-Frequency Perspectives on Hybrid Cloud-to-Ground Lightning Observed by the FORTE Satellite

Michael Peterson[1], Tracy E. L. Light[1], Xuan-Min Shao[1]

[1]ISR-2, Los Alamos National Laboratory, Los Alamos, New Mexico

Corresponding author: Michael Peterson (mpeterson@lanl.gov), B241, P.O. Box 1663 Los Alamos, NM, 87545

Key Points:

- The FORTE satellite included optical and RF payloads for measuring transient signals, including a CCD imager based on the design used with OTD/LIS/GLM
- Flash cluster data is produced for FORTE that includes fast photodiode and RF events incorporated into the cluster feature data tree
- Optical / RF measurements are used to examine cloud pulses, the return stroke, and subsequent K-changes in an oceanic hybrid CG flash

LA-UR 20-28458

Abstract

We use the coincident optical and radio-frequency measurements taken by the FORTE satellite to shed light on common optical signatures recorded by NASA and NOAA lightning imagers during Cloud-to-Ground (CG) lightning. We build flash cluster data for FORTE using the same clustering techniques as GLM and document the optical / RF evolution of an oceanic hybrid -CG flash over its 656 ms duration. The flash began with strong VHF emission from a Narrow Bipolar Event (NBE) that initiated a period of normal bilevel intracloud (IC) activity in two vertical layers (8 km and 12 km) that lasted for 490 ms. VHF waveforms show step leader activity ahead of seawater attachment in the return stroke. All impulsive VHF sources after the stroke come from the lower (8 km layer) only. K-changes are noted following the return stroke, but no subsequent strokes are detected.

The optical flash began 136 ms after the NBE RF pulse. 22 of the 30 optical groups were dim and occurred during the in-cloud phase of the flash. This activity included both isolated pulses and sustained periods of illumination over tens of milliseconds. Initial cloud pulses accounted for 23% of the total optical radiance from the flash. Illumination during the return stroke contributed a further 58% of the total radiance, and the K-changes and cloud pulses after the stroke supplied the remaining 19%. These results highlight the benefit of having RF alongside optical lightning measurements for clarifying signatures in the optical data and providing information on their physical origins.

Plain Language Summary

Lightning has been measured from space for more than 25 years. Most space-based sensors were optical instruments that detect lightning by looking for the cloud-top lighting up. Recent studies have shown that we can measure how lightning moves using this type of instrument, but distinguishing strokes from radiant intracloud processes on a one-to-one basis is still an unsolved problem.

Radio lightning measurements provide greater insights into the physical origin of lightning signals, and one satellite flew with both optical and radio lightning sensors. We use data collected by this FORTE satellite to investigate the link between physical lightning processes (CG, in-cloud impulsive events, K-changes) and their optical signals. We confirm many of the findings from previous studies, but also show that making inferences with optical data alone can be problematic. Only optical and radio measurements, combined, provide a complete picture of what is going on in the lightning flash and how the flash illuminates the cloud.

1 Introduction

The Geostationary Lightning Mapper (GLM: Goodman et al., 2013) on NOAA's current-generation Geostationary Operational Environmental Satellite (GOES) provides an unprecedented continuous view of lightning activity across the Americas and a large fraction of the Pacific Ocean. While ground-based long-range lightning detection networks report mainly Cloud-to-Ground (CG) strokes (see Cummins and Murphy, 2009 for an overview of what different types of networks can sense), space-based lightning imagers like GLM detect total lightning - CG strokes plus intracloud (IC) discharges. Optical lightning imagers achieve total lightning detection by measuring transient changes in cloud-top illumination. Any physical process that lights up the cloud can be detected by GLM, not just powerful attachments to the Earth's surface during CG strokes.

We have demonstrated that lightning imagers are capable of detecting weak optical emissions from leader development and K-processes (Peterson et al., 2017a), including those that are simultaneous with certain Transient Luminous Events (TLEs) such as gigantic jets (Boggs et al., 2019). Moreover, because these instruments consist of pixelated Charge-Coupled Device (CCD) arrays, they can be used to map the spatial evolution of individual lightning flashes over time (Peterson et al., 2018) and identify truly exceptional lightning events (Peterson et al., 2017b; Peterson et al., 2020a; Peterson and Kirkland, 2020; Peterson and Lay, 2020). These observations have proven particularly useful for documenting lightning outside of the convective core (Peterson and Liu, 2011; Peterson et al., 2020b) that tends to have a complex lateral structure (Figures 6-8 in Peterson, 2019a).

GLM and similar instruments are a powerful tool for studying lightning physics on scales that exceed the line-of-sight domains of ground-based Very High Frequency (VHF) band

Lightning Mapping Arrays (LMAs: Rison et al., 1999) and interferometer / optical whole sky systems (Mazur et al., 1995, 1998). Space-based sensors further extend coverage to remote areas of the world where ground-based measurements are impractical - including the open ocean. There are two key limitations to space-based optical lightning measurements, however. First, they provide limited information about the emissions source. Lightning imagers only measure where clouds light up and by how much. Second, the lightning signals that make it to orbit have been modified substantially by the intervening cloud layer between the source and the sensor through scattering and absorption. The more exotic flash footprints measured by the Lightning Imaging Sensor (LIS) and GLM suggest that there is as much information about the cloud scene embedded within the lightning radiance data as there is about the flash (i.e., Peterson et al., 2017a,b; Peterson, 2019b).

Due to the optical scattering effects in both space- and ground-based data, and a lack of un-scattered optical measurements to serve as truth, there are large uncertainties inherent in any attempt to infer a lightning discharge type on the basis of optical lightning data alone (Davis et al., 2002; Koshak, 2010). For this reason, our recent analyses of optical phenomenology (particularly Peterson and Rudlosky, 2019) have resisted making firm connections between optical signatures and the physical processes that have traditionally been identified through Radio-Frequency (RF) waveform analyses.

A comprehensive view of lightning from multiple types of measurements is required to understand the evolution of lightning signals over the duration of the flash. In this study, we use the wealth of coincident optical and VHF-band RF measurements provided by the Fast On-Orbit Recording of Transient Events (FORTE) satellite to identify the physical origins of common optical phenomena in the OTD, LIS and GLM datasets. We focus on lightning that produces

particularly large and radiant optical pulses that are consistent with return strokes from Koshak (2010). Future work will examine other distinctive signatures including lateral flash development.

2 Data and Methodology

The FORTE satellite was launched into Low Earth Orbit (LEO) in mid-1997. It had the same 70º inclination angle as the MicroLab-1 satellite that hosted NASA's Optical Transient Detector (OTD: Christian et al., 2003), but at a higher ~825 km orbit than OTD (710 km altitude). Two key differences between FORTE and the NASA / NOAA instruments are: (1) FORTE's coincident RF measurements that provide additional insights into transient lightning emissions, and (2) FORTE being operated in campaign mode with instrument settings, collection strategies, and trigger modes adjusted on-orbit. The coincident optical / RF data collected by FORTE and its variety of operating modes create a niche for FORTE research that complements lightning research with NASA's LIS and OTD, and NOAA's GLM instruments.

We use these combined optical / RF measurements to construct a new cluster feature FORTE dataset similar to the LIS / OTD science datasets or the GLM operational data product. This dataset (described in Section 2.3) encompasses all FORTE observations including the various operating modes of the individual instruments. However, we only analyze one lightning flash from this dataset in the present study. For this reason, we describe only the FORTE instruments and operating modes relevant to this case in Sections 2.1 and 2.2. See Jacobson et al. (1999) for a detailed description of the FORTE RF payloads and Suszcynsky et al. (2000, 2001)

for the optical payloads. Furthermore, Light (2020) provides a comprehensive review of the FORTE mission and its novel scientific findings.

2.1 The FORTE Optical Lightning System

The FORTE Optical Lightning System (OLS) operated from late 1997 until early 2010 and consisted of two separate optical lightning detectors. The Lightning Locating System (LLS) was a CCD lightning imager based on a modified version of the LIS/OTD design (Suszcynsky et al., 2001). The key role of the LLS was geolocating lightning activity. The LLS had an 80° square field of view across the CCD array that resulted in a ~10 km pixel size (similar to OTD). The LLS frame rate was 405 FPS, which was lower than the nominal (500 FPS) and average on-orbit (558 FPS) LIS frame rates (Bitzer and Christian, 2015). This design choice increased lightning event detection while reducing event splitting between consecutive frames. The issue of multiple lightning pulses contributing to events is not critical to FORTE, however, (as it was for LIS / OTD) due to the availability of coincident high-speed instrumentation that could identify individual pulses within a single LLS integration frame.

The second optical instrument was a photodiode detector (PDD) that provided broadband (0.4 μm – 1.1 μm) fast (66,667 FPS) measurements of optical pulses from lightning over a large field of view (Kirkland et al., 2001; Suszcynsky et al., 2001). The PDD record length and trigger settings were reconfigured throughout the FORTE mission. The PDD data that we consider were collected while the instrument was configured to have a record length of 1.92 ms and an autonomous noise-riding amplitude threshold trigger. In the autonomous PDD trigger mode, the optical signals must exceed the average background radiance for a specified duration (usually 5 samples or 75 μs) to trigger the instrument (Suszcynsky et al., 2000; Suszcynsky et al., 2001).

This limits triggering on energetic particle impacts, for example when the spacecraft was over the South Atlantic Anomaly (SAA). There is also a finite number of PDD triggers that can be captured on flash time scales. The maximum trigger count depends on the PDD configuration and is usually a multiple of 10. During the time period where the flash of interest occurred, the PDD was recording a maximum of 20 events per flash. This can cause flashes with substantial in-cloud activity at the beginning of the flash to exhaust the available PDD triggers before the return stroke occurs. We will show later on that this occurred with the flash of interest and, as a result, the early development of the flash is well-resolved but the return stroke and later activity is not captured by the PDD.

2.2 The FORTE Radio Frequency System

FORTE recorded RF transients from late 1997 until 2003. The FORTE RF system consisted of two identical Log-Periodic Antennas (LPAs) mounted orthogonal to each other along FORTE's 10-m nadir-pointing boom, and three broadband receivers that operated in the 26 to 300 MHz range (Jacobson et al., 1999; Suszcynsky et al., 2000; Shao and Jacobson, 2001; Light et al., 2001a). The RF system had a 120° effective field of view that covered a ~6,000 km diameter footprint on the surface of the Earth. Two of the three RF receivers comprise the TATR payload that we use in this study. Each TATR receiver (designated TATR/A and TATR/B) sampled one of the FORTE antennas at 50 megasamples per second (Shao and Jacobson, 2002). The TATR receivers could be independently tuned to cover a desired 22 MHz subband. The length of TATR records and the ratio of samples before and after the trigger were also commandable. The TATR data that we consider had 800 μs record lengths with 200 μs of pretrigger data, and TATR/A and TATR/B both set to record lowband (26 – 48 MHz) signals.

2.3 FORTE flash cluster data for combined optical / RF lightning measurements

Since LLS events are not clustered into features representing flashes or thunderstorms during the original FORTE data processing, we generate our own LLS lightning cluster features here. The techniques used to construct cluster feature data are described at length in the LIS/OTD/GLM literature (Christian et al., 2000; Mach et al., 2007; Goodman et al., 2010). We choose to adapt the clustering technique used with GLM (Goodman et al., 2010) to produce an integrated FORTE lightning cluster feature dataset that establishes family links between LLS, PDD and RF detections.

In the standard clustering hierarchy used by NASA and NOAA, the basic unit of lightning detection is termed an "event." On pixelated optical sensors such as LIS, OTD or GLM, an event corresponds to a single pixel on the CCD array being triggered during a single 2-ms integration frame. The FORTE literature uses a different definition for an LLS "event" that permits detection across multiple integration frames. We use the NASA / NOAA convention here and extract the triggered pixels from each frame in such cases to define unique events. We also apply this event definition to PDD and RF detections by considering the entire FOV of these instruments to be one "pixel" and the variable triggering intervals to be one "frame." The triggering interval is the minimum period of time until another trigger is possible, and includes the record length plus any post-trigger dead time.

These modifications allow us to construct a general lightning cluster feature hierarchy that can be applied to all FORTE instruments. The parent-child relationships between feature levels and typical time domains are depicted in Figure 1. The data tree extends from microsecond-scale "sample" features up through minute-scale "area" features that will be

defined below. We use this general template to fill out the full hierarchy of cluster features for each FORTE instrument.

We start describing these features at the "event" level (Figure 1d) that is defined for all FORTE instruments and represents a unique trigger. Moving up from the event level, the next most complex feature is the "group." Groups comprise contiguous portions of the instrument FOV that produce events during a single frame. For this reason, they share the same panel as events in Figure 1d. In the case of LLS, groups might contain multiple illuminated pixels whose sides or corners touch on the CCD array. For the PDD and RF system (that contain just one "pixel"), groups are identical to events.

Groups that occur close to one another in space and time are clustered into features describing lightning flashes. Flash features (Figure 1b) are defined by applying a Weighted Euclidian Distance (WED) model to the geolocated position and time displacements of groups (Mach et al., 2007; Goodman et al., 2010). As with GLM, we use 16.5 km as the X and Y distance thresholds and 330 ms as the time threshold. However, we choose to apply the WED model to group centroids (as is done with LIS) rather than to group constituent event positions. We do this to prevent overclustering - where highly-radiant pulses leading to very large groups can merge all nearby concurrent lightning into a single flash.

The feature level between groups and flashes – "series" (Figure 1c) - requires flash clustering in its derivation. Series features describe periods of sustained illumination from lightning. Groups that (1) occur in consecutive frames or that have just one empty frame between them and (2) are assigned to the same flash feature will be clustered into the same series feature.

Finally, area features (Figure 1a) describe thunderstorm snapshots during the FORTE overpass. Areas are constructed by applying the group-to-flash clustering model (with no time displacement term) to the flash centroid positions rather than the group centroid positions.

All of the features described above are computed for each FORTE instrument – LLS, PDD, and the RF system. However, the PDD and RF system are both capable of constructing features at finer time scales than events. PDD and RF records have a granularity on the order of microseconds rather than milliseconds. We refer to the basic units of PDD and RF measurements as "samples" (Figure 1f). We also define an intermediate "pulse" feature (Figure 1e) that is comprised of multiple sequential samples within a single optical or RF event where the signal exceeds the background average radiance (PDD) or power (TATR) by a specified threshold. For this study, we specify that threshold to be one standard deviation above the mean background value.

Certain feature levels are either not reported by some of the FORTE instruments or are identical to other features in the clustering hierarchy for the same instrument. Table 1 lists the features that are available to each instrument and shades the features that are most useful for analyzing lightning activity. The features from each instrument (in each vertical column in Table 1) are linked via direct parent-child relationships. We also cross-link features from different instruments by establishing "step-parent / step-child" relationships between higher-level features from one instrument and lower-level features from another. For example, an LLS flash can be the step-parent of a PDD event or RF pulse. The differing FOVs for the OLS (80°) and RF system (120°) complicate the cross-linking because the RF system can detect events outside of the LLS / PDD domain. To mitigate this issue, we adopt the Total Electron Content (TEC) matching methodology from Jacobson et al., (1999) to screen for RF events that traverse a

different slant path through the ionosphere than the RF signals from the OLS flash in question. In the following analyses, we will show all events that occurred in the same time frame as the flash of interest and then exclude specific RF events that originated from elsewhere in the TATR FOV.

3 Results

The goal of this study is to investigate the physical lightning processes that lead to common optical signatures observed during LLS (and, by extension, LIS/OTD/GLM) flashes. Associations between optical phenomena and physical processes are generally made by observing such a process on the ground (i.e., continuing current from Bitzer, 2017 or gigantic jets from Boggs et al., 2019) and then going back to the space-based lightning imager data to determine (1) if it detected anything, and (2) whether the recorded signatures are consistent with our understanding of the physics involved in such a process. If the instrument triggered and produced a sufficiently unique optical signature, then the whole lightning imager record is searched to find similar candidates for the process of interest.

We take the opposite approach here. We first look through our millions of FORTE flashes to find cases that represent unique optical signatures, and then use the RF instrumentation on FORTE to investigate what type of process produced the optical signals. This study focuses on the very large and bright groups that may be return strokes in CG flashes (Koshak, 2010). A case of oceanic lightning is identified that contains an exceptionally-radiant group that illuminated a large cloud-top area – on the same scale as the extreme cases of LIS flashes presented in Peterson et al. (2017b).

3.1 Overview of FORTE measurements during an oceanic CG flash on 10/13/1999

The selected case was observed over the Coral Sea northeast of Australia on 10/13/1999. It produced 33 LLS groups clustered into 24 series over its 656 ms duration. Most groups were dim optical pulses with the longest series lasting 19-ms. There were three particularly-radiant groups that reached at least one standard deviation (sigma) above the mean group energy. The largest of these bright groups illuminated a cloud-top area of 3864 km^2 during a single LLS frame. In total, the LLS observed 120 events associated with this flash while the PDD recorded 20 events (its maximum trigger count) and TATR recorded 73 events.

LLS Flash Extent Densities (FED: Lojou and Cummins, 2004) and trigger rates are plotted in Figure 2 for the 15-minute window surrounding the flash. FED (Figure 2a) increments once for every distinct lightning flash that illuminates a given grid point, regardless of how many times that point is illuminated during the flash. It thus combines flash rate and flash extent into a single gridded product. The FED plot indicates that the overall storm was neither extensive nor organized. Lightning was broadly-scattered over the region and occurred at low rates. It is thus likely that the optical footprint of the flash of interest was large (3864 km^2) because light was able to illuminate nearby clouds, as we often see with LIS (Peterson and Liu, 2013; Peterson et al., 2017a).

The trigger rate plot in Figure 2b counts the number of OLS, PDD, and TATR RF events from 7.5 minutes before the flash to 7.5 minutes after the flash. Note that the time axis is not linear, but accelerates near the zero line that represents the window encompassing the LLS flash duration. Event rates are rather low before the flash at less than 10 per minute in most bins. TATR and the PDD both trigger in the minute leading up to the flash, but there are no triggers of any kind between 1 s and 0.33 s before its first LLS group. There are a few TATR triggers that occur in the 1-second period after the flash, but none of these triggers have optical events

associated with them. Though these subsequent RF events could result from continued flash activity that LLS does not resolve, we stop our analysis at LLS final light. With such low trigger rates, we can be reasonably confident that our selected flash of interest is responsible for the PDD and TATR events over the LLS flash duration, but we will verify this by comparing the TEC measurements from the TATR events later on.

3.2 Evolution of optical signals from the flash

The evolution of LLS groups and events over the flash duration is shown in Figure 3. A plan view is plotted in the central panel (Figure 3c) with total CCD pixel energy shown as a color contour plot. Line segments depicting the spatial progression of groups from first light (dark grey) to final light (light grey) are overlaid. The panel above the plan view (Figure 3a) shows the longitude extent of each group in the flash, while the panel to the right (Figure 3d) shows latitude extent. Figure 3b contains a histogram of group energy presented as a sigma level (i.e., the number of standard deviations above or below the mean group energy for the flash). Finally, the two panels below the plan view show timeseries of group area (Figure 3e) and group energy (Figure 3f).

The two isolated events to the north of the flash footprint stand out as possible artifacts. They both occur in the same LLS integration frame (364 ms after first LLS light), but are clustered into separate flash features. This frame is important because it also contains the largest and second-brightest group in the flash of interest (Figure 3e,f). Because these pixels do not light up at any other point during the flash window, they may simply be reflections of the most radiant pulse from the flash.

Figures 3e and f show that the LLS recorded 23 dim groups over the course of 350 ms starting at LLS first light. This activity is then followed by a single series containing the two largest and most energetic groups in the flash. After a lull for ~70 ms, the third bright group occurs immediately following a low-energy group. Only two additional LLS groups are recorded during the remaining 200 ms of the flash. Both final groups are brighter than the initial 23 groups, but they still have only ~10% of the radiance of the brightest group in the flash.

A first-order assessment of the optical flash without taking any other data into consideration might be that the first groups describe in-cloud events during initial leader development that culminate in peak optical emission at return stroke seawater attachment (near 362 ms in Figures 3e, f). The stroke lights up for two LLS frames due to either frame splitting (i.e., the trigger time was at the end of the first group) or continuing current. There are two total series that contain bright groups at the 1-sigma level, resulting in an optical multiplicity of two and an interseries interval of 74 ms. The final LLS groups could be subsequent strokes or K-changes. However, we cannot make any stronger inferences from the optical data, alone.

3.3 Combined optical and RF assessment of flash evolution

Fortunately, we do not have just the optical data to work with. The flash produced 73 TATR events over its duration that allow us to investigate what physical lightning processes are occurring when light is detected by the LLS and PDD. Figure 4 shows timeseries of LLS groups, and PDD and TATR events over the course of the flash. The time domain is expanded to include the 200 ms before LLS first light in order to capture the initial RF events that did not have coincident LLS or PDD triggers. Optical energy is shown in Figure 4a for LLS and Figure 4b for PDD as a percent of the maximum group energy reported by each instrument. Optical energies

are plotted on a logarithmic scale to facilitate comparison with RF TATR event peak powers in Figure 4c. After "dechirping" (correcting for ionospheric dispersion) and "prewhitening" (suppressing narrowband carrier waves, for example from radio transmissions) the TATR records returned for each event (these methods are summarized in Light et al., 2020), we calculate the average power across the TATR band for each sample and then report the maximum band-averaged RF power for all samples that are grandchildren of the event (see Table 1). Event peak powers are expressed in dB relative to the strongest RF emissions recorded over the flash window (duration +/- 330 ms) in Figure 4c. All subsequent RF powers are reported following this convention.

TATR pulse data are primarily used to classify the types of RF emissions from the flash based on recognizable features in the TATR waveform data. The fractions of pulses in each 2-ms window in Figure 4 that are isolated impulses (single peaks), single intracloud pulse pairs (Trans-Ionospheric Pulse Pairs – TIPPs: Holden et al., 1995), pulse trains containing multiple TIPPs, or diffuse / mixed (i.e., a diffuse pulse with impulsive peaks superimposed on the broad waveform) are shown in Figure 4d. RF events that did not contain any perceptible pulses are classified as single instances of "sustained featureless emission" per event.

TIPPs in VHF waveforms recorded from space result from in-cloud discharges where the first peak that reaches the satellite comes from the direct line-of-sight detection of the RF pulse and the second peak comes from the reflection of the pulse off the Earth's surface (Jacobson et al., 1999). For each TIPP case, we measure the time difference between the two pulses and use the positions of the satellite and the nearest geolocated LLS group to estimate the altitude of the in-cloud source. The altitudes of all TIPPs in the flash are plotted in Figure 4e. Finally, Figure 4f

integrates the LLS group radiance and TATR antenna response (in V^2 m^{-2}) over time to quantify how the received optical and RF signals accumulated over the flash duration.

There are similarities between the overall optical evolution of the LLS flash shown in Figure 3 and the evolution of the TATR flash shown in Figure 4c. The optical and RF flashes both start out with a period of frequent weak triggers leading up to the most radiant LLS group. We use TATR waveform analysis (Suszcynsky et al., 2000; Light et al., 2001) to conclude that this energetic optical pulse was caused by a first negative return stroke. Optical and RF timeseries from this event will be shown in Section 4.3.

The RF sources are primarily impulsive in-cloud events before the return stroke and then diffuse K-change events afterwards (Figure 4d). There is a total of 103 impulsive in-cloud pulse features in the 73 TATR events plus an additional 6 pulse features associated with the return stroke and another 18 from diffuse K-changes. The impulsive in-cloud features are clustered into two layers: a lower layer at 8 km altitude, and an upper layer at 12 km altitude. The TEC values returned from the dechirping algorithm are nearly identical (65±5 TECU) for all but two TATR waveforms (not shown). Thus, 71 of the TATR events traversed the same slant path through the ionosphere and came from the flash of interest. These two outlier events occurred at +14 ms and +530 ms in Figure 4c and were the second and third most powerful RF pulses recorded during the flash. Their reported TEC values were 110±5 TECU and 140±5 TECU (i.e., twice the TEC experienced by the remaining RF signals – likely due to a relatively horizontal slant angle to the satellite). We ignore these outlier events in subsequent analyses.

The TATR observations from the flash are consistent with ground-based VHF findings from interferometer systems and LMA networks. Negative breakdowns in positive-polarity

charge regions radiate strongly in the VHF band measured by these ground-based systems, while breakdowns in negative charge regions tend to be weaker. For this reason, Rison et al., (1999) suggested that the relative difference in source counts between the upper and lower layers in a bilevel flash is sufficient to determine the polarity of the breakdown and the charge regions involved. In our case, most of the in-cloud sources preceding the return stroke come from the upper layer (i.e., only 4 lower-layer sources occur from -200 ms to 250 ms). This suggests a bilevel IC breakdown in a normal-polarity thunderstorm with a negative charge region at 8 km altitude and a positive charge region at 12 km altitude.

While the period before the return stroke was characterized by frequent dim LLS groups, the period following the return stroke only contained a small number of highly-radiant groups. While most of the impulsive IC events in the flash came from the upper layer, no impulsive sources were observed from this layer after +364 ms. Thus, the cessation of dim cloud pulses in the LLS data coincides with the upper layer appearing to become cut off. This may be due to increased attenuation experienced by the optical signals from the lower layer. When most RF activity in our case is coming from the upper charge layer closer to the cloud top (first LLS light until just before the return stroke) we have 41 RF events in forty 2-ms windows (Figure 4d) compared to 24 total LLS groups. The trigger rate of LLS relative to TATR during this time period is thus ~60%. For the period following the return stroke when the upper layer is quiet (368 ms until the end of the LLS flash), there are 4 LLS groups compared to 14 TATR triggers in 11 2-ms windows. During this period, LLS triggers 28% of the time that TATR triggers, or in ~36% of the 2-ms frames where TATR reports an event.

The optical and RF measurements of the flash also differ in their initial triggers. The LLS flash begins with its lowest-radiance trigger at 0 ms. The PDD did not trigger alongside the LLS

until the radiance reaches around twice the radiance of this first LLS group (or 2% of the maximum LLS group radiance for the flash). As a result, the start of the PDD flash is delayed by 40 ms relative to LLS. The TATR flash, on the other hand, precedes LLS first light by 136 ms and begins with a single isolated impulsive in-cloud event that is followed by trains of cloud pulses. This event was the most powerful RF event in the flash and waveform analysis indicates that it resulted from a Narrow Bipolar Event (NBE). NBEs - also termed Compact Intracloud Discharges (CIDs) - are quick in-cloud events that have comparable currents to return strokes (~10 kA), but whose extents inferred from ground-based measurements are small – between 0.3 km and 1 km (Smith et al., 1999). NBEs are an example of "dark lightning" (Light and Jacobson, 2002; Jacobson et al., 2013) since they typically do not produce enough light (or perhaps no light at all) to trigger optical instruments despite generating some of the most powerful natural RF emissions on Earth.

We divide the hybrid CG flash into four phases based on its RF phenomenology: the initial NBE (-136 ms), normal IC development following the NBE (-135 ms to 354 ms), the return stroke (355 ms to 367 ms), and subsequent K-changes and in-cloud pulses following the return stroke (368 ms to 800 ms). Each of these periods is discussed in depth below.

4 Discussion

4.1 Initial NBE

The flash of interest began with 6 TATR events in the 330 ms period leading up to first LLS light (Figure 2b, Figure 4c). The first RF trigger occurred 136 ms before first LLS light and was an isolated in-cloud event. This event was an example of the high-power impulsive in-cloud lightning events discussed in the FORTE literature (Smith et al,. 1999; Jacobson et al., 1999;

Light and Jacobson, 2002) that have been shown to be associated with NBEs (i.e., Rison et al., 2016; Eack, 2004; Smith et al., 1999). These events are among the most powerful VHF lightning sources (LeVine, 1980) and occur at altitudes ranging from 6 km to 15 km (Light and Jacobson, 2002). See Rison et al. (2016) for a review on NBEs.

NBEs / CIDs can occur in relative isolation (Smith et al., 1999), or as the first VHF pulse that sets off a normal IC flash (Rison et al., 1999). A National Lightning Detection Network (NLDN: Cummins et al., 1998) analysis of CID events suggests that 73% are isolated while 24% occur before, during, or after "normal" lightning, and the remaining 4% occur in pairs separated by no more than 200 ms (Nag et al., 2010).

The NBE at -136 ms occurred near the lower charge later at 9 km altitude and began a period of normal in-cloud activity that lasted for 400 ms. This TATR event was the strongest RF emitter recorded during the flash - even compared to the return stroke. It contributed 9% of the total received RF energy for the flash (Figure 4f) despite being an impulsive event. Even with this strong RF emission, it was not optically bright enough to trigger the LLS or PDD - which is typical of NBEs (Light and Jacobson, 2002).

4.2 Normal IC activity

The normal IC activity following the NBE produced regular TATR triggers with an average interval of 9 ms between successive events. All but 4 triggers from -135 ms to +354 ms (just before the return stroke) were low-power TIPPs and pulse pair trains from normal IC breakdowns. This IC phase was the most active period during the flash and contained 22 out of

33 LLS groups, all 20 PPD events, and 48 out of 73 TATR events. The PDD exhausted its available triggers within the first 300 ms of the LLS flash. LLS optical emissions during this period were between 1% and 10% of the peak LLS radiance during the return stroke. In total, the IC phase of the flash contributed 22% of the received RF energy and 23% of the optical LLS radiance from the flash. This apparent agreement between optical and RF is probably coincidental since TATR triggered regularly for 52 ms before first LLS light, and the accumulation of optical energy is relatively piecemeal compared to the nearly constant rate at which RF signals accumulated after the CID.

The first 100 ms of the flash is shown in LLS evolution plot in Figure 5. Figure 5 is identical to Figure 3, but with OLS group (greyscale by group number) and PDD sample (blue) energy depicted on a logarithmic scale in panel (e), and TATR sample RF power (blue) shown in panel (f). There were 4 LLS groups in the first 100 ms of the LLS flash. The two that consisted of 2 events also triggered the PDD, while the 2 single-event groups did not. The first group in the flash was also the dimmest at just 1% the maximum group energy. PDD triggering on multi-pixel LLS groups continued for the next 112 ms in the flash duration (not shown).

The optical and RF events during the first 212 ms of the LLS flash are all isolated in time with TATR and the PDD waveforms describing impulsive sources. Figure 6 shows the next period of the flash that included sustained optical emission over an extended period of time. The longest LLS series in the flash lasted 19 ms (8 LLS frames) starting at +247 ms. However, this LLS series is part of a longer period of consecutive PDD triggers that started at +220 ms and ended at +278 ms. Despite the dead time between records (approximately equal to the record length) and impulsive peaks notable in the blue PDD light curve in Figure 6e, the flash appears to have been generating sustained optical emission the whole time as the LLS groups / events

started to expand westward in Figure 6c. The LLS groups during this period were generally dim (< 1σ in Figure 6b), and periods where PDD triggered but LLS did not suggest that the sources were not spatially concentrated enough to trigger individual LLS pixels.

4.3 Return stroke

Optical and RF signals during the 12-ms window encompassing the return stroke are shown in Figure 7. Starting with TATR trigger at +358 ms, the flash produced the constantly-strengthening sustained featureless emission associated with stepped leader development ahead of a first negative return stroke (Light et al., 2001a) over a 4.5 ms period. Seawater attachment occurred at +362 ms and the strong narrow VHF peak was accompanied by the most radiant LLS group in the flash.

The VHF emissions surrounding the return stroke accounted for 21% of the overall TATR antenna response, but the optical emissions accounted for 58% of the total flash energy recorded by LLS (Figure 4f). The evolution plot for this period is shown in in Figure 7a-d. The optical emissions are divided into 6 groups in two LLS frames. Because multiple groups occur in each of these two frames, the groups become overlaid in Figure 7e, resulting in only three distinct entries being notable in the group radiance timeseries.

The two largest groups both have radiances above the 3-sigma level in Figure 7b. Lines are not drawn connecting these groups to the preceding group-level structure of the flash in Figure 7c due to the large distances separating them from the nearest preceding group, but their positions can still be noted in Figure 7a and d. Two of these groups occur within the flash

481 footprint in Figure 7c, while the remaining two occur north of the flash. Because these pixels did
482 not light up at any other time, we speculate that they are reflections rather than coincident
483 lightning activity.

484 The two isolated groups that occur within the flash footprint are distinct because only a
485 portion of the 4751 km^2 flash footprint is illuminated during each LLS frame. The western half
486 of the flash is illuminated in the first frame along with an isolated event to the east (Figure 7a),
487 and then the eastern portion of the flash footprint is illuminated in the second frame along with
488 an isolated western event. This second bright group is less radiant than the first, but has the
489 largest group area at 3864 km^2 (81% of the overall flash footprint area).

490 Because the eastern and western portions of the flash footprint are illuminated in separate
491 LLS frames, there are pixels – even near the flash center – that are illuminated during one group
492 and not the other. Since no subsequent groups are observed, we can conclude that the LLS glint
493 filter was not activated and that the flash likely did not have prolonged continuing current.
494 However, there are also pixels within the flash footprint that were not illuminated during either
495 frame associated with the return stroke. The three black pixels in Figure 7c form a hole in the
496 middle of an otherwise-contiguous feature on the LLS CCD array. We have noted this behavior
497 before with LIS flashes (Figure 1 in Peterson and Liu, 2013 is one example) where coincident
498 radar data show that such optical holes correspond to dense convective cells embedded in the
499 flash footprint that seem to block radiance from reaching the satellite. Dark pixels causing
500 “holes” in otherwise contiguous flash footprints during intense low-altitude processes provides
501 further evidence that clouds modify the optical signals recorded from orbit – even to the point of
502 preventing detection. The pixels corresponding to the hole were illuminated during earlier

503 periods of the flash dominated by high-altitude IC pulses (including in Figure 6c), and thus the
504 hole is not observed in Figure 3c.

505

506 4.4 Post-RS K-changes and IC pulses

507 The final phase of the flash describes the K-changes and in-cloud pulses following the
508 return stroke. In-cloud activity was limited to the lower (8 km) charge layer and dominated by K-
509 processes. Four LLS groups were detected, but no subsequent strokes were identified in the
510 TATR waveform data. This final period provided the remaining 19% of optical energy in the
511 flash and the final 47% of the total TATR response. These TATR signals were supplied by
512 diffuse VHF events that produced broad RF pulses. Three such TATR events in the 75-ms period
513 following the return stroke did not trigger the LLS. However, a particularly strong and long-
514 lasting K-change occurred at +440 ms that was followed by strong optical emission. The VHF
515 and optical measurements from this period are shown in Figure 8. The TATR antenna response
516 integrated over the waveform for this trigger was 24% greater than the return stroke, and it
517 produced the third-brightest LLS group. As with the in-cloud pulses preceding the return stroke,
518 there was no hole in this group – the K-change illuminated the entire convective core of the
519 parent thunderstorm.

520 This group was also the only group outside of the series encompassing the return stroke
521 to reach the 1-sigma radiance level and thus advance the optical multiplicity. The fact that it was
522 caused by a K-change rather than a subsequent stroke justifies our previous aversion to drawing
523 parallels between the traditional RF-based multiplicity parameter and our new optical
524 multiplicity parameter (Peterson and Rudlosky, 2019). The optical multiplicity is simply a

measure of how many times a flash lights up the clouds above a reference value based on weak cloud pulses, and can capture radiant processes other than strokes.

5 Conclusion

Coincident optical and RF measurements from the FORTE satellite are used to examine the joint evolution of an oceanic CG lightning flash. The first signals received during the flash window (330 ms before first light until 330 ms after final light) included an apparent NBE (-136 ms) that set off a period of regular RF triggering on impulsive in-cloud events. This period of normal IC activity lasted for 490 ms until the beginning of stepped leader activity ahead of the return stroke. Cloud pulses were clustered into an upper layer at 12 km altitude and a lower layer at 8 km altitude, consistent with a bilevel hybrid CG flash. The relative frequency of RF triggering in the two layers suggests that the storm had a normal charge structure and the CG flash was of negative polarity. Cloud pulses are noted in only the lower layer following the return stroke, and are accompanied by diffuse RF emissions from K-changes.

The optical flash began 52 ms after the NBE. The initial IC phase of the flash produced 22 of its 30 optical groups. These groups were generally weak, varying between 1% and 10% of the peak group energy for the flash, and contributed 23% of the total flash radiance. There were no such weak triggers during the 4.5 ms of stepped leader activity leading up to the return stroke. The most radiant optical groups occurred upon attachment over the course of 2 LLS integration frames (~5 ms). The bright group in the first frame was the most energetic in the flash, while the bright group in the second frame was dimmer with a larger area. The next LLS group occurred 74 ms later during a K-change event. No subsequent strokes were observed in the VHF waveform data.

These results demonstrate how coincident space-based optical and RF measurements can be used to construct a comprehensive view of lightning that is more informed than the perspectives from either measurement type in isolation. RF measurements confirm the physical origin of optical signals and document events that are too optically dim to be detected from space. Optical measurements provide geolocation information for RF events and highlight periods of sustained current flow in both CG and IC phases of the flash. Our analyses support the idea that large and bright groups result from return strokes, but also that radiant processes like K-changes similarly stand out above the baseline emissions from the flash. While the value of instruments such as GLM for investigating lightning physics in flashes across the hemisphere cannot be overstated, there is a significant benefit to taking a data fusion approach between available optical and RF measurements to prevent mis-associations and gain a clearer picture of what is going on.

Acknowledgments

Los Alamos National Laboratory is operated by Triad National Security, LLC, under contract number 89233218CNA000001. The data presented in this study are located at Peterson (2020).

References

Bitzer, P. M., 2017: Global distribution and properties of continuing current in lightning, *J. Geophys. Res. Atmos.*, **122**, 1033–1041, doi:10.1002/2016JD025532

Bitzer, P.M. and H.J. Christian, 2015: Timing Uncertainty of the Lightning Imaging Sensor. *J. Atmos. Oceanic Technol.*, **32**, 453–460, https://doi.org/10.1175/JTECH-D-13-00177.1

570 Boggs, L. D., N. Liu, M. Peterson, S. Lazarus, M. Splitt, F. Lucena, A. Nag, and H. Rassoul, 2019: First
571 observations of gigantic jets from geostationary orbit. *Geophys. Res. Lett.*, **46**.
572 https://doi.org/10.1029/2019GL082278
573 Budden, K. G., 1985: The Propagation of Radio Waves. *Cambridge Univ. Press*, New York
574 Cecil, D. J., D. E. Buechler, and R. J. Blakeslee, 2014: Gridded lightning climatology from TRMM-LIS and OTD:
575 Dataset description. *Atmos. Res.*, **1350136,** 404-414
576 Christian, H. J., R. J. Blakeslee, S. J. Goodman, and D. M. Mach (Eds.), 2000: Algorithm Theoretical Basis
577 Document (ATBD) for the Lightning Imaging Sensor (LIS), NASA/Marshall Space Flight Center,
578 Alabama. (Available as http://eospso.gsfc.nasa.gov/atbd/listables.html, posted 1 Feb. 2000)
579 Christian, H. J., R. J. Blakeslee, D. J. Boccippio, W. L. Boeck, D. E. Buechler, K. T. Driscoll, S. J. Goodman, J. M.
580 Hall, W. J. Koshak, D. M. Mach, and M. F. Stewart, 2003: Global frequency and distribution of lightning
581 as observed from space by the Optical Transient Detector. *J. Geophys. Res.*, **108**(D1), ACL-4.
582 Cummins, K. L., M. J. Murphy, E. A. Bardo, W. L. Hiscox, R. B. Pyle, and A. E. Pifer, 1998: A combined
583 TOA/MDF technology upgrade of the U.S. National Lightning Detection Network. *J. Geophys. Res.*, **103**,
584 9035–9044
585 K. L. Cummins and M. J. Murphy, 2009: An Overview of Lightning Locating Systems: History, Techniques, and
586 Data Uses, With an In-Depth Look at the U.S. NLDN, *IEEE Tramn. on Electromag. Compat.*, **51**, 3, pp.
587 499-518, doi: 10.1109/TEMC.2009.2023450.
588 Eack, K. B. (2004), Electrical characteristics of narrow bipolar events, *Geophys. Res. Lett.*, **31**, L20102,
589 doi:10.1029/2004GL021117.
590 Goodman, S. J., D. Mach, W. J. Koshak, and R. J. Blakeslee, 2010: GLM Lightning Cluster-Filter Algorithm
591 (LCFA) Algorithm Theoretical Basis Document (ATBD). NOAA NESDIS Center for Satellite
592 Applications and Research. (Available as https://www.goes-
593 r.gov/products/ATBDs/baseline/Lightning_v2.0_no_color.pdf, posted 24 Sept. 2010)
594 Goodman, S. J., R. J. Blakeslee, W. J. Koshak, D. Mach, J. Bailey, D. Buechler, L. Carey, C. Schultz, M. Bateman,
595 E. McCaul Jr., and G. Stano, 2013: The GOES-R geostationary lightning mapper (GLM). *J. Atmos. Res.*,
596 **125-126**, 34-49

597 Holden, D. N., C. P. Munson, and J. C. Devenport, 1995: Satellite observations of transionospheric pulse pairs,
598 Geophys. Res. Lett., **22**, 889–892
599 Jacobson, A. R., S. O. Knox, R., Franz, and D. C. Enemark, 1999: FORTE observations of lightning radio-frequency
600 signatures: Capabilities and basic results. *Radio Sci.*, **34** (2), 337– 354, doi:10.1029/1998RS900043
601 Jacobson, A. R., K. L. Cummins, M. Carter, P. Klingner, D. Roussel-Dupré, and S. O. Knox, 2000: FORTE radio-
602 frequency observations of lightning strokes detected by the National Lightning Detection Network. *J.*
603 *Geophys. Res.*, **105** (D12), 15653– 15662, doi:10.1029/2000JD900103
604 Jacobson, A. R., and X.-M. Shao, 2002: FORTE satellite observations of very narrow radiofrequency pulses
605 associated with the initiation of negative cloud-to-ground lightning strokes. *J. Geophys. Res.*, **107** (D22),
606 4661, doi:10.1029/2001JD001542
607 Jacobson, A. R., T. E. L. and Light, 2003: Bimodal radio frequency pulse distribution of intracloud-lightning signals
608 recorded by the FORTE satellite. *J. Geophys. Res.*, **108**, 4266, doi:10.1029/2002JD002613, D9
609 Jacobson, A. R., Light, T. E. L., Hamlin, T., & Nemzek, R. (2013). Joint radio and optical observations of the most
610 radio-powerful intracloud lightning discharges. *Annales Geophysicae (09927689)*, *31*(3).JPL, 2019: Global
611 Ionospheric Maps. Accessed 7 May 2019, https://iono.jpl.nasa.gov/gim.html
612 Koshak, W. J., 2010: Optical characteristics of OTD flashes and the implications for flash-type discrimination. *J.*
613 *Atmos. Oceanic. Technol.*, **27,** 1,822 – 1,838
614 Le Vine, D. M. (1980). Sources of the strongest RF radiation from lightning. *Journal of Geophysical Research:*
615 *Oceans*, *85*(C7), 4091-4095.
616 Light, T. E., D. M. Suszcynsky, and A. R. Jacobson, 2001a: Coincident radio frequency and optical emissions from
617 lightning, observed with the FORTE satellite. *J. Geophys. Res.*, **106** (D22), 28223– 28231,
618 doi:10.1029/2001JD000727
619 Light, T. E., D. M. Suszcynsky, M. W. Kirkland, and A. R. Jacobson, 2001: Simulations of lightning optical
620 waveforms as seen through clouds by satellites. *J. Geophys. Res.*, **106** (D15), 17103– 17114,
621 doi:10.1029/2001JD900051
622 Light, T. E. L., and A. R. Jacobson, 2002: Characteristics of impulsive VHF lightning signals observed by the
623 FORTE satellite. *J. Geophys. Res.*, **107** (D24), 4756, doi:10.1029/2001JD001585

624 Lojou, J.-Y., K. L. Cummins, 2004: On the representation of two- and three-dimensional total lightning information.
625 In Preprints, Conference on Meteorological Applications of Lightning Data (pp. Paper 2.4, AMS Annual
626 Meeting, San Diego, CA, USA)
627 Mach, D. M., H. J. Christian, R. J. Blackeslee, D. J. Boccippio, S. J. Goodman, and W. L. Boeck, 2007:
628 Performance assessment of the Optical Transient Detector and Lightning Imaging Sensor. *J. Geophys. Res.,*
629 ***112***, D09210
630 Massey, S. R., S. O. Knox, R. C. Franz, D. N. Holden, and C. T. Rhodes, 1998: Measurements of transionospheric
631 radio propagation parameters using the FORTE satellite. *Radio Sci.*, **33**, 1739–1753
632 Mazur, V., P. R. Krehbiel, and X.-M. and Shao, 1995: Correlated high-speed video and radio interferometric
633 observations of a cloud-to-ground lightning flash. *J. Geophys. Res.*, **100** (D12), 25731– 25753,
634 doi:10.1029/95JD02364
635 Mazur, V., X.-M. Shao, and P. R. Krehbiel, 1998: "Spider" lightning in intracloud and positive cloud-to-ground
636 flashes. *J. Geophys. Res.*, **103** (D16), 19811– 19822, doi:10.1029/98JD02003
637 Nag, A., V. A. Rakov, D. Tsalikis, and J. A. Cramer, 2010: On phenomenology of compact intracloud lightning
638 discharges. *J. Geophys. Res.*, **115**, D14115, doi:10.1029/2009JD012957
639 Peterson, M., 2019a: Research applications for the Geostationary Lightning Mapper operational lightning flash data
640 product. *J. Geophys. Res.*, **124**, 10205– 10231. https://doi.org/10.1029/2019JD031054
641 Peterson, M., 2019b: Using lightning flashes to image thunderclouds. *J. Geophys. Res.*, **124**, 10175– 10185.
642 https://doi.org/10.1029/2019JD031055
643 Peterson, M., 2020, CIERRA-FORTE Flash Cluster Data, https://doi.org/10.7910/DVN/63FWWU, Harvard
644 Dataverse, DRAFT VERSION
645 Peterson, M. J. and C. Liu, 2011: Global statistics of lightning in anvil and stratiform regions over the tropics and
646 subtropics observed by TRMM, *J. Geophys. Res.*, **116**, D23, doi: 10.1029/2011JD015908
647 Peterson, M. J. and C. Liu, 2013: Characteristics of lightning flashes with exceptional illuminated areas, durations,
648 and optical powers and surrounding storm properties in the tropics and inner subtropics, *J. Geophys. Res.*,
649 **118**, 11,727-11,740, doi: 10.1002/jgrd.50715
650 Peterson, M. J., W. Deierling, C. Liu, D. Mach, C. Kalb, 2017a: The properties of optical lightning flashes and the
651 clouds they illuminate. *J. Geophys. Res. Atmos.*, **122**, 423–442, doi:10.1002/2016JD025312

652 Peterson, M. J., S. Rudlosky, and W. Deierling, 2017b: The evolution and structure of extreme optical lightning
653 flashes. *J. Geophys. Res. Atmos*., **122**, doi: 10.1002/2017JD026855
654 Peterson, M., S. Rudlosky, and W. Deierling, 2018: Mapping the Lateral Development of Lightning Flashes from
655 Orbit. *J. Geophys. Res. Atmos.*, **123**, 9674– 9687. https://doi.org/10.1029/2018JD028583
656 Peterson, M., S. Rudlosky, 2019: The time evolution of optical lightning flashes. *J. Gephys. Res.*, **124**, 333– 349.
657 https://doi.org/10.1029/2018JD028741
658 Peterson, M. J., Lang, T. J., Bruning, E. C., Albrecht, R., Blakeslee, R. J., Lyons, W. A., et al., 2020a: New World
659 Meteorological Organization certified megaflash lightning extremes for flash distance (709 km) and
660 duration (16.73 s) recorded from space. *Geophys. Res. Lett.*, **47**, e2020GL088888.
661 https://doi.org/10.1029/2020GL088888
662 Peterson, M., S. Rudlosky, and D. Zhang, 2020b: Thunderstorm Cloud-Type Classification from Space-Based
663 Lightning Imagers. *Mon. Wea. Rev.*, **148**, 1891–1898, https://doi.org/10.1175/MWR-D-19-0365.1.
664 Rison, W., R.J. Thomas, P.R. Krehbiel, T. Hamlin, and J. Harlin, 1999: A GPS-based three-dimensional lightning
665 mapping system: initial observations in central New Mexico. *Geophys. Res. Lett*., **26**, 23, 3573-3576.
666 Shao, X.-M., 2018: Broadband RF Interferometric Mapping and Polarization (BIMAP) observations of Mini-
667 Discharges in thunderstorms. AGU Fall Meeting 2018, Washington, DC, Amer. Geophys. Union.
668 https://agu.confex.com/agu/fm18/meetingapp.cgi/Paper/422277
669 Shao, X.-M., and A. R. Jacobson, 2001: Polarization observations of broadband VHF signals by the FORTE
670 satellite. *Radio Sci.*, **36** (6), 1573– 1589, doi:10.1029/2000RS002600
671 Shao, X.-M., and A. R. Jacobson, 2002: Polarization observations of lightning-produced VHF emissions by the
672 FORTE satellite, *J. Geophys. Res*., **107** (D20), 4430, doi:10.1029/2001JD001018
673 Smith, D. A., X.-M. Shao, D. N. Holden, C. T. Rhodes, M. Brook, P. R. Krehbiel, M. Stanley, W. Rison, and R. J.
674 Thomas, 1999: A distinct class of isolated intracloud lightning discharges and their associated radio
675 emissions. *J. Geophys. Res.*, **104** (D4), 4189– 4212, doi:10.1029/1998JD200045
676 Suszcynsky, D. M., M. W. Kirkland, A. R., Jacobson, R. C. Franz, S. O. Knox, J. L. L. Guillen, and J. L. Green,
677 2000: FORTE observations of simultaneous VHF and optical emissions from lightning: Basic
678 phenomenology. *J. Geophys. Res.*, **105** (D2), 2191– 2201, doi:10.1029/1999JD900993

679 Suszcynsky, D. M., T. E. Light, S., Davis, J. L., Green, J. L. L. Guillen, and W. Myre, 2001: Coordinated
680 observations of optical lightning from space using the FORTE photodiode detector and CCD imager. *J.*
681 *Geophys. Res.*, **106** (D16), 17897– 17906, doi:10.1029/2001JD900199

682

683 **Table 1.** A **t**abular representation of the parallel tree data structures that describe lightning cluster features for each
684 FORTE instrument. Useful features for analyzing lightning flashes are shaded. Note the vertical offsets due to
685 relevant time scales varying by instrument
686

Time Scale	OLS		RFS	
	LLS	PDD	TATR	HUMR
10^3 s	VIEWTIME	VIEWTIME	VIEWTIME	VIEWTIME
10^2 s	AREA	AREA	AREA	AREA
10^1 s	BACKGROUND	BACKGROUND	BACKGROUND	BACKGROUND
10^0 s	FLASH	FLASH	FLASH	FLASH
10^{-1} s				
10^{-2} s	SERIES	SERIES	SERIES	SERIES
10^{-3} s	GROUP / EVENT	GROUP / EVENT	GROUP / EVENT	GROUP / EVENT
10^{-4} s		PULSE		
10^{-5} s		SAMPLE	PULSE	PULSE
10^{-6} s			SAMPLE	SAMPLE
10^{-7} s				

687
688
689

690

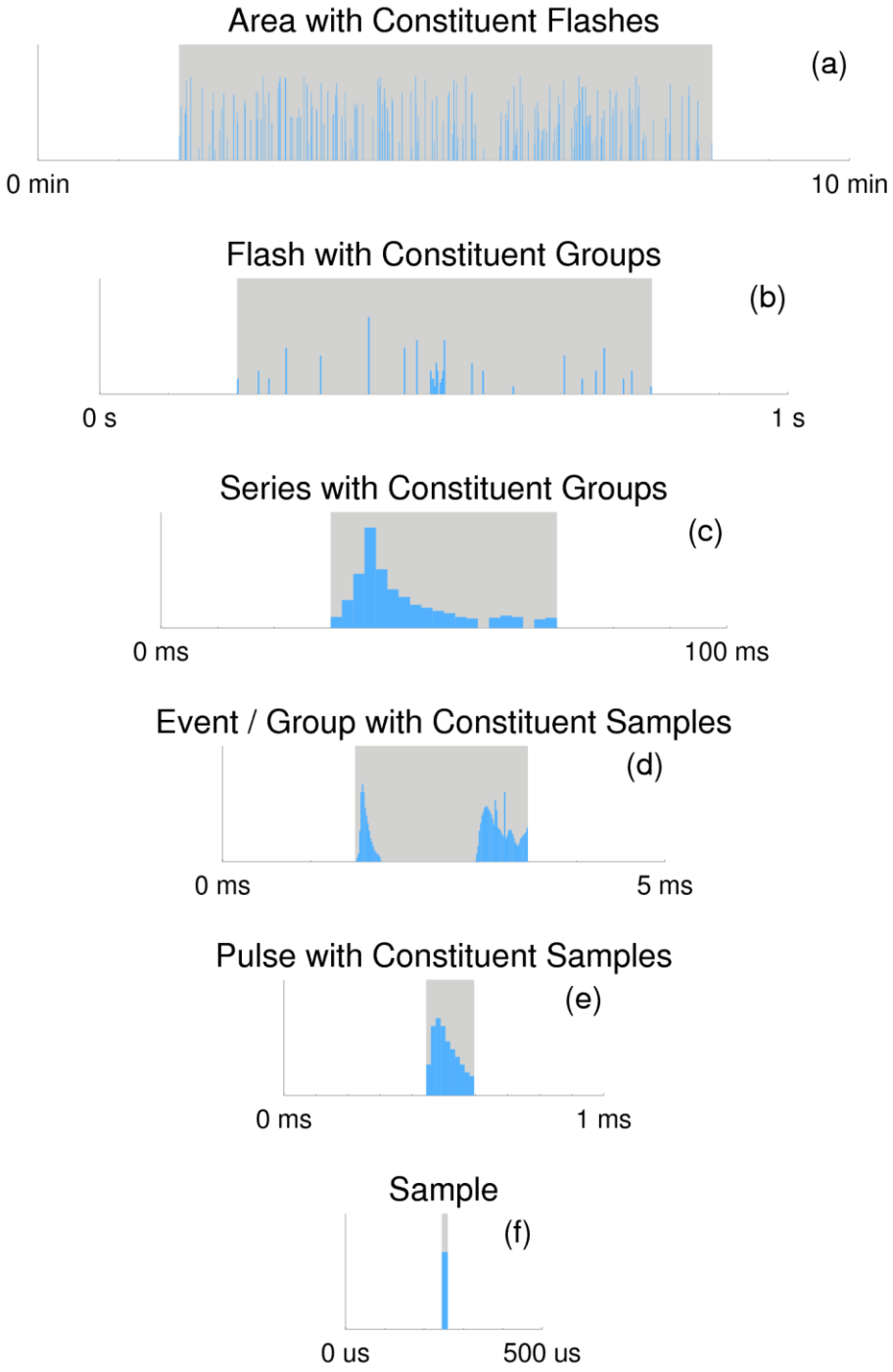

691
692
693 **Figure 1.** The general lightning cluster feature hierarchy used for all FORTE instruments and the time domain
694 associated with each feature. Features are the parents of features above them on the diagram and children of the
695 features below them. The grey boxes show the domain of the current feature at each level while constituent lower-
696 level features are shaded blue.
697
698

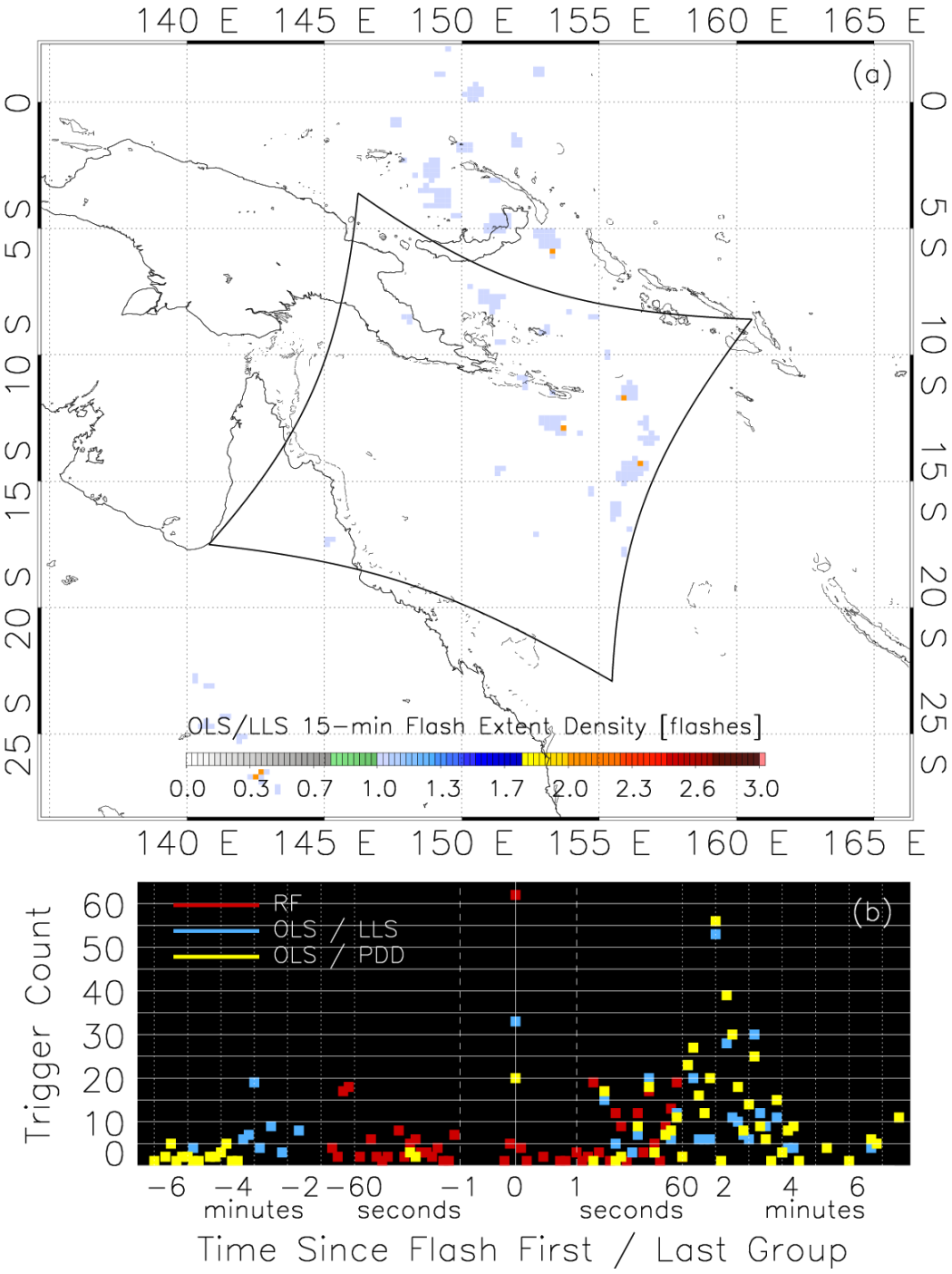

Figure 2. FORTE LLS lightning activity close to the flash of interest. (a) FED across the LLS FOV and (b) optical and RF trigger rates during the 15-minute window surrounding the flash. Because lightning was infrequent across the FORTE FOV during the flash window, signals from other flashes are unlikely. (Should you mark on the map the interested flash?)

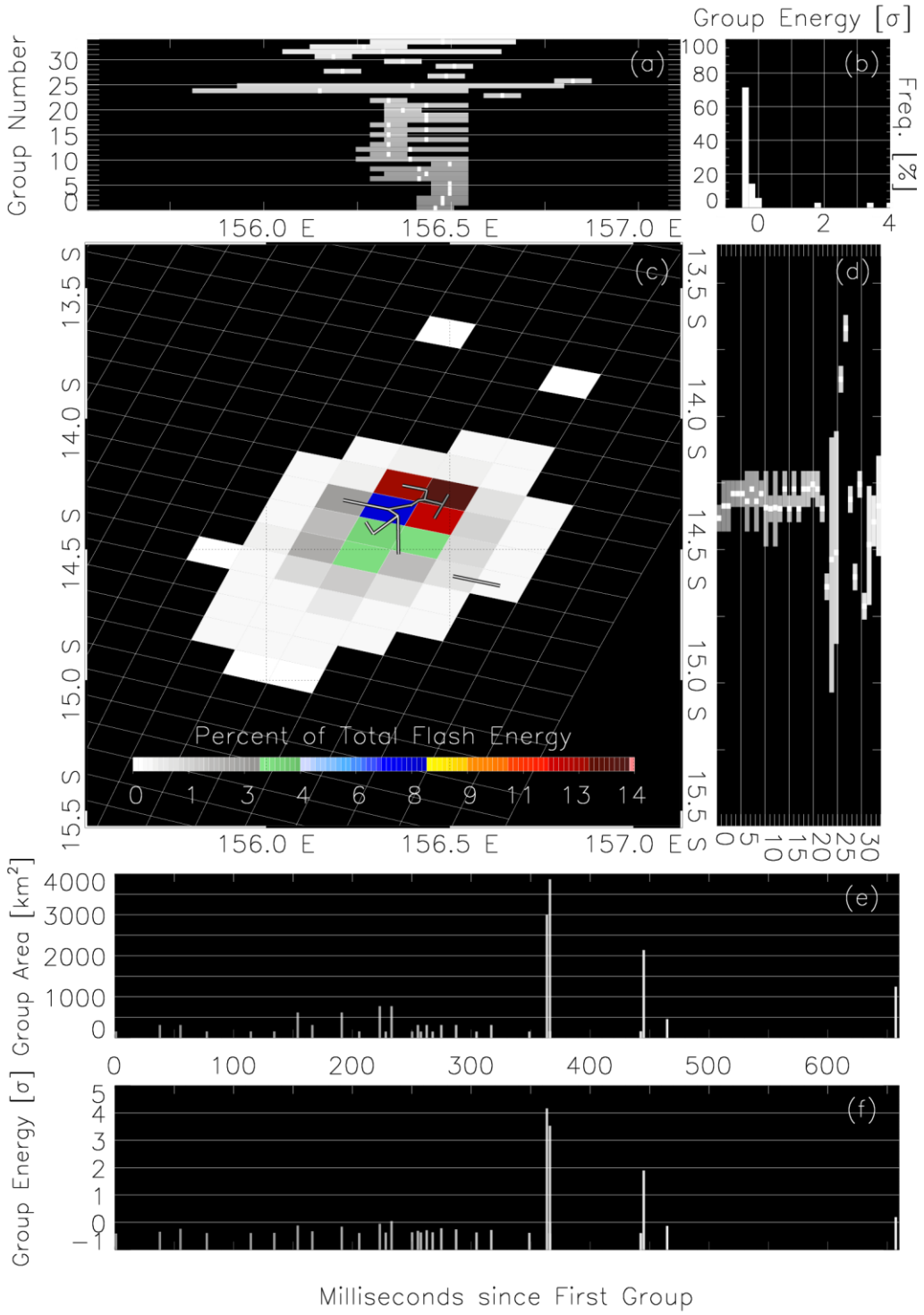

Figure 3. Evolution plot for the LLS flash. (a) group extent by longitude, (b) group energy distribution, (c) plan view of flash energy (color contour) and group extent (line segments), (d) group extent by latitude, (e) timeseries of group area, and (f) timeseries of group energy. Group energies are expressed as a sigma level relative to the average group energy in the flash. The greyscale in all plots represents the sequential group index.

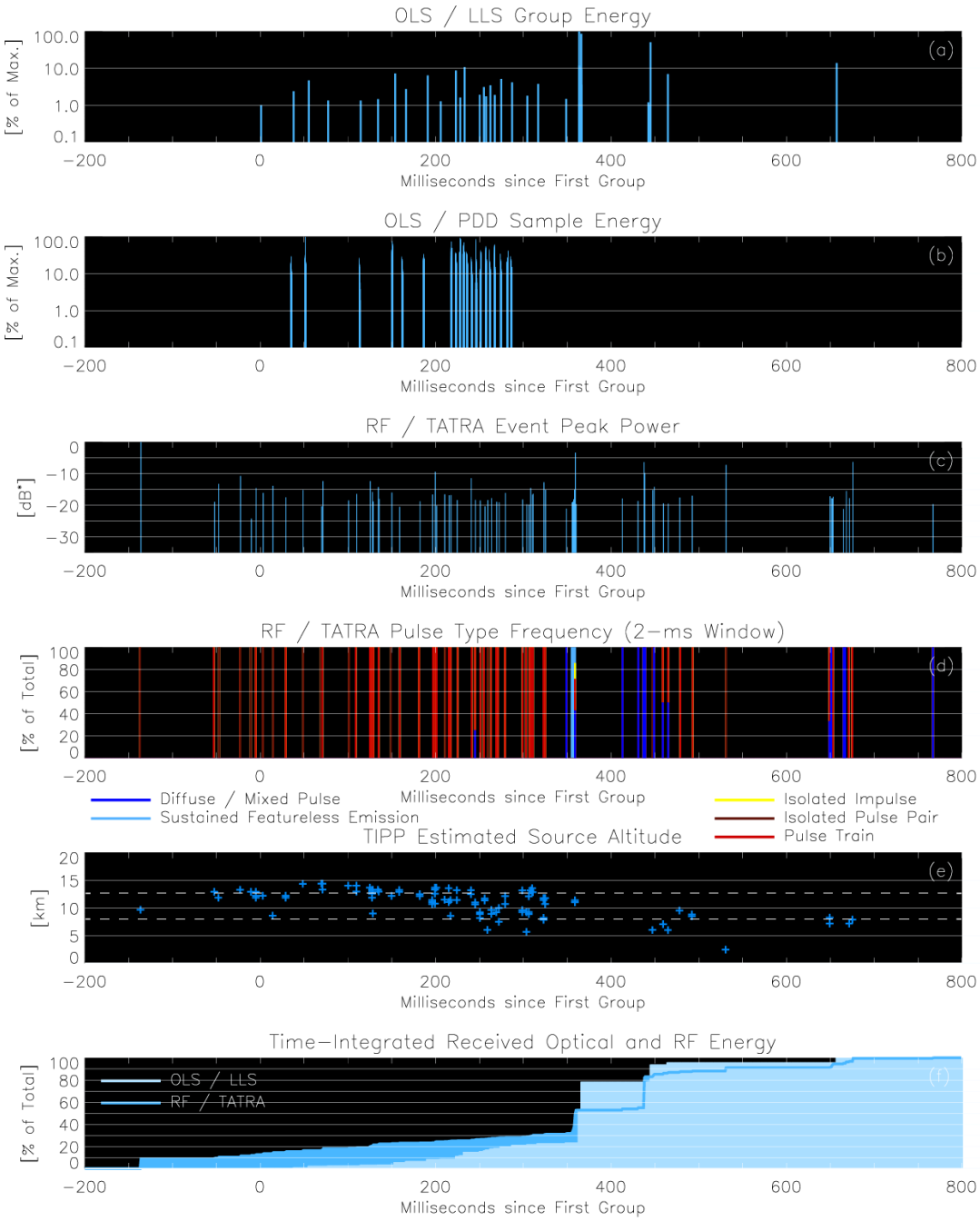

Figure 4. Timeseries showing the combined optical / RF evolution of the flash. (a) LLS and (b) PDD optical energies. (c) TATR RF power (* signifies relative to the overall peak RF power during the flash window). (d) TATR pulse classification shown as the frequency of each pulse type in a 2-ms window. (e) estimated altitude of in-cloud (TIPP) sources. (f) time-integrated optical and RF energies over the flash duration

721

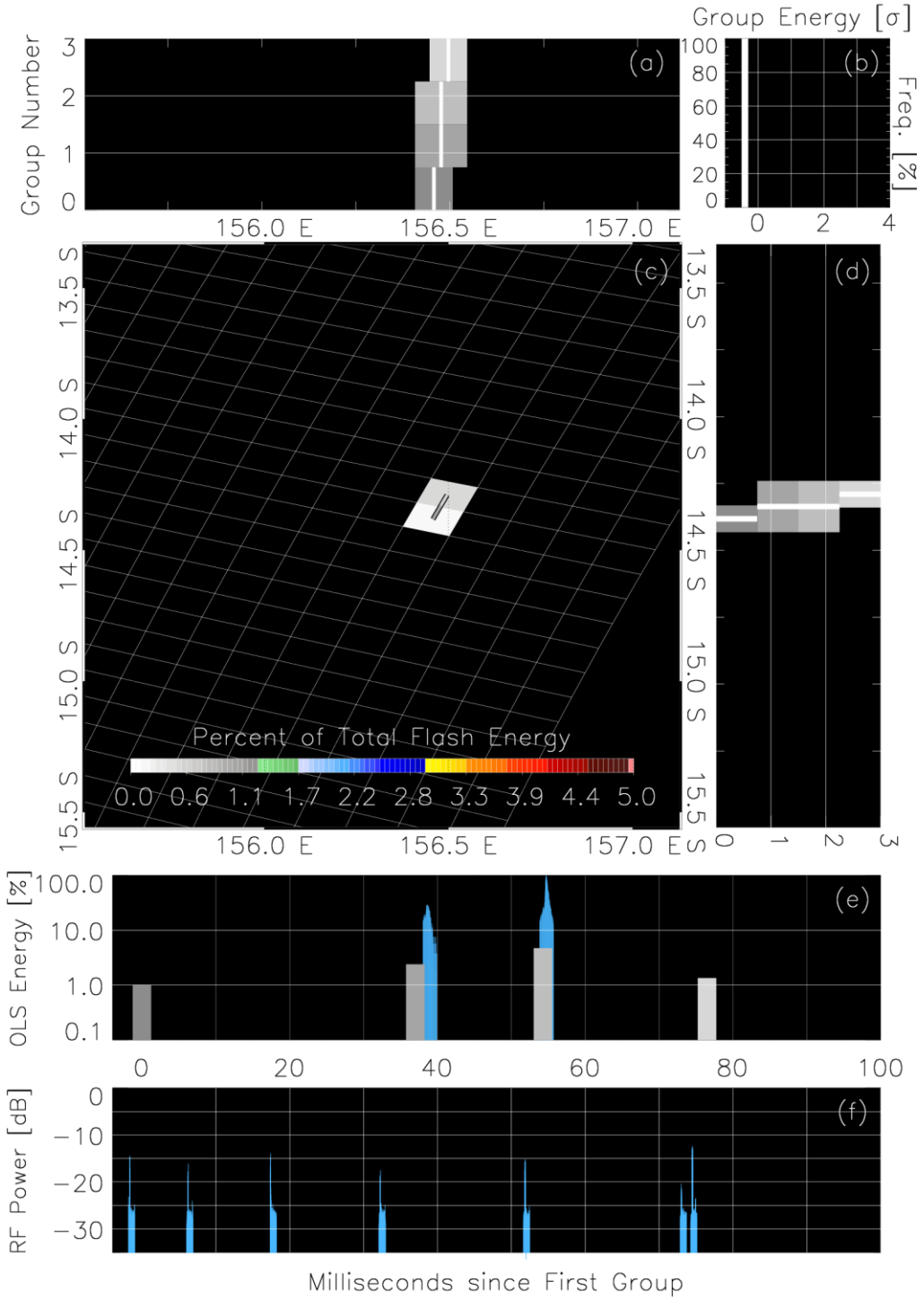

722
723
724 **Figure 5.** Evolution plot for the first 100 ms of optical triggers in the flash. Identical to Figure 3, but with LLS
725 group area replaced by TATR RF power in (f) and PDD data plotted blue in (e).
726
727

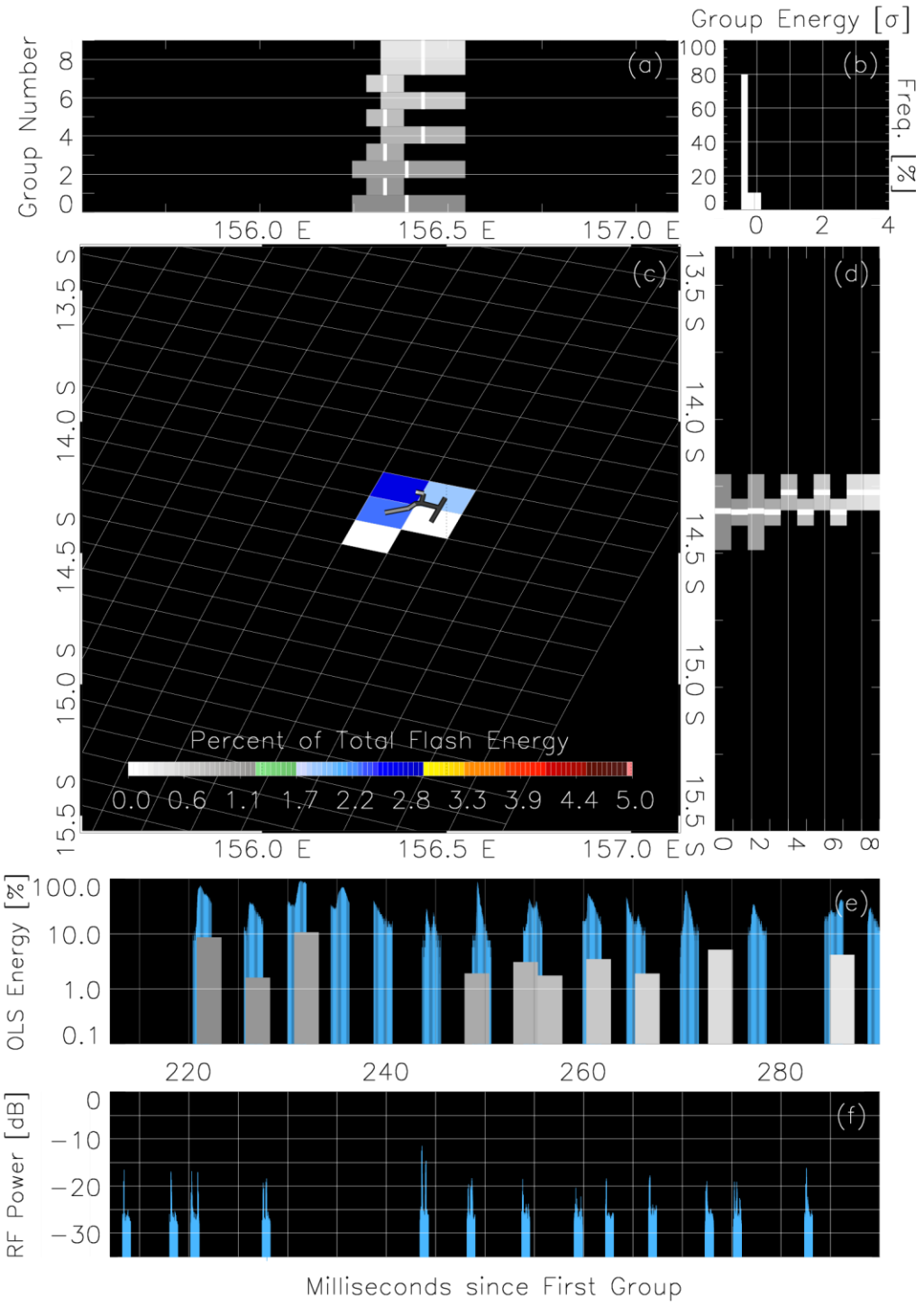

Figure 6. Same as Figure 5, but for the period 212 ms – 290 ms that encompasses a long-lasting PDD series.

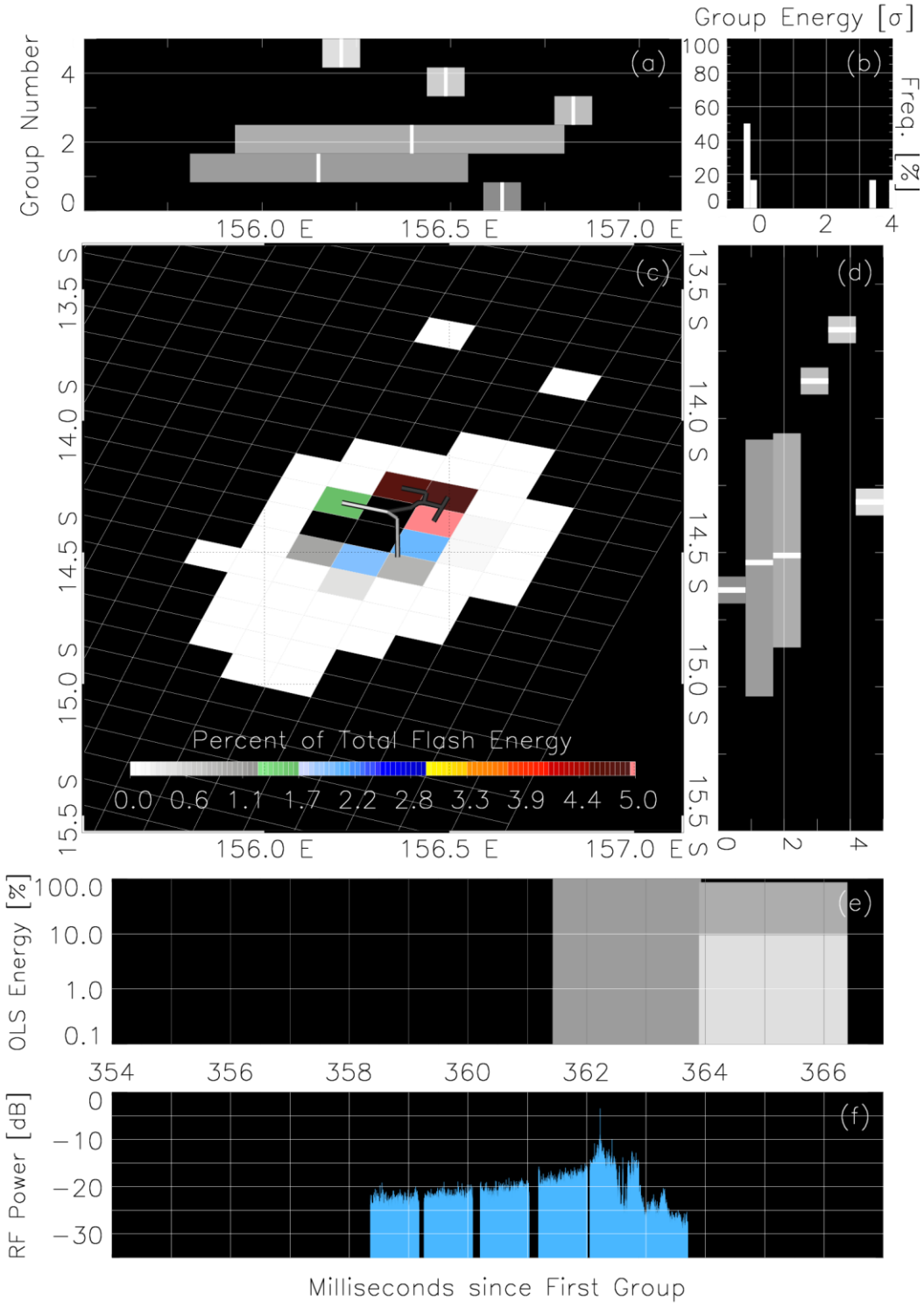

Figure 7. Same as Figure 5, but for the period 354 ms – 367 ms that contains the return stroke.

737

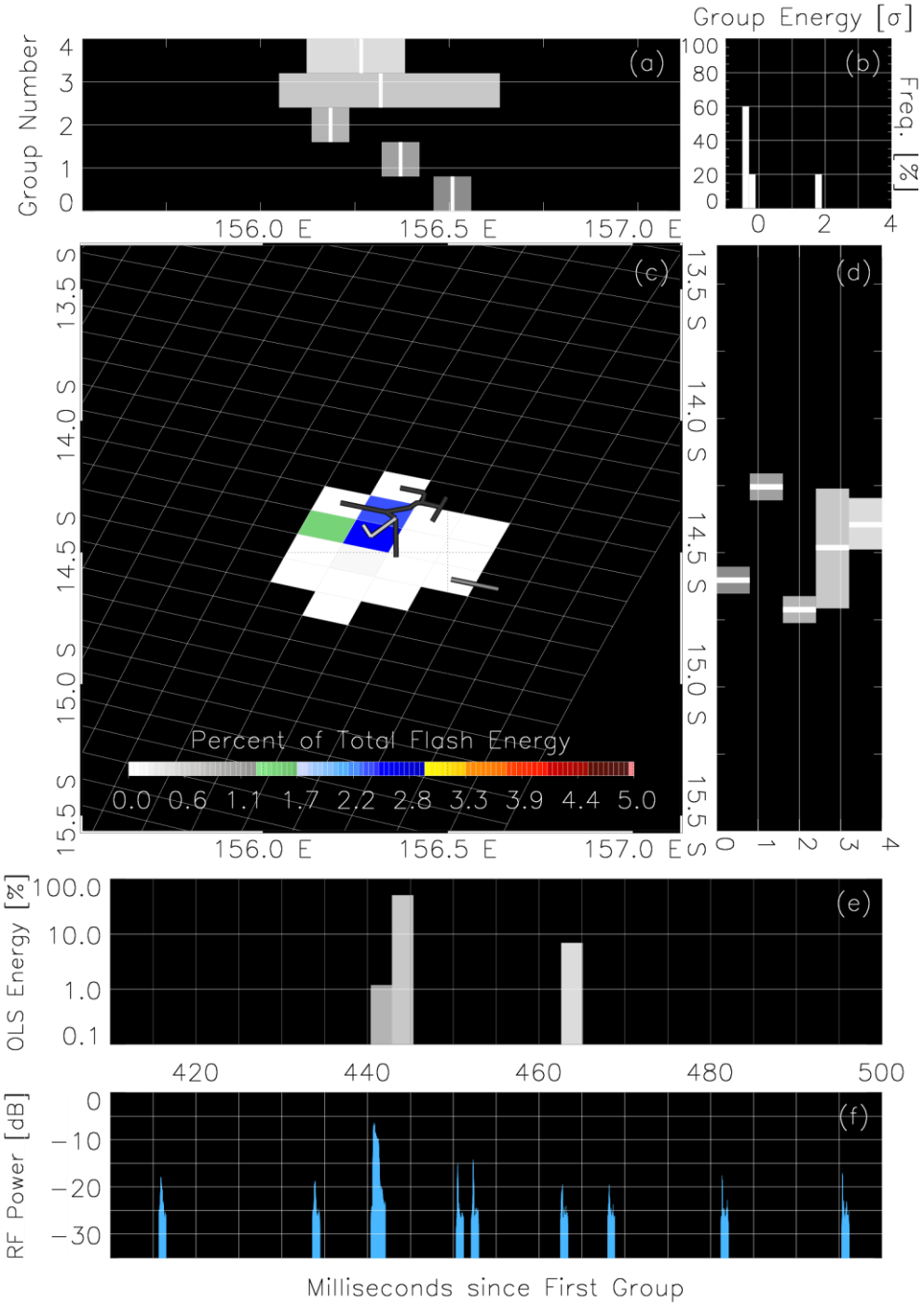

738
739
740 **Figure 8.** Same as Figure 5, but for the period 410 ms – 500 ms that contains the final bright LLS group.
741
742

743

Figure 1.

Area with Constituent Flashes

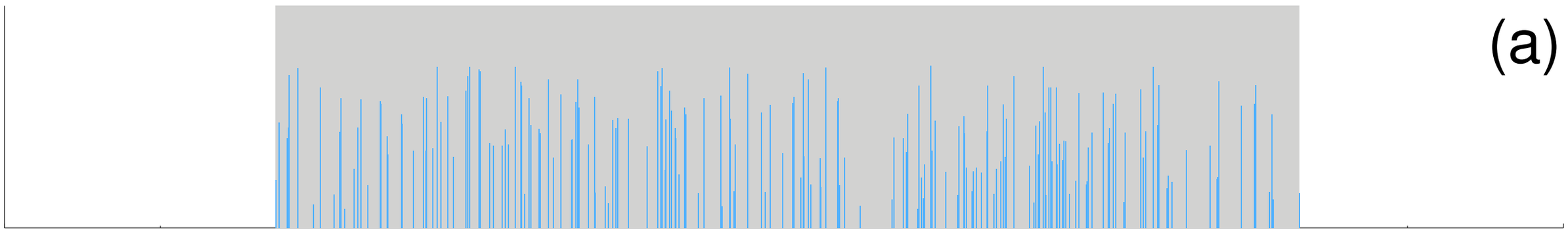

Flash with Constituent Groups

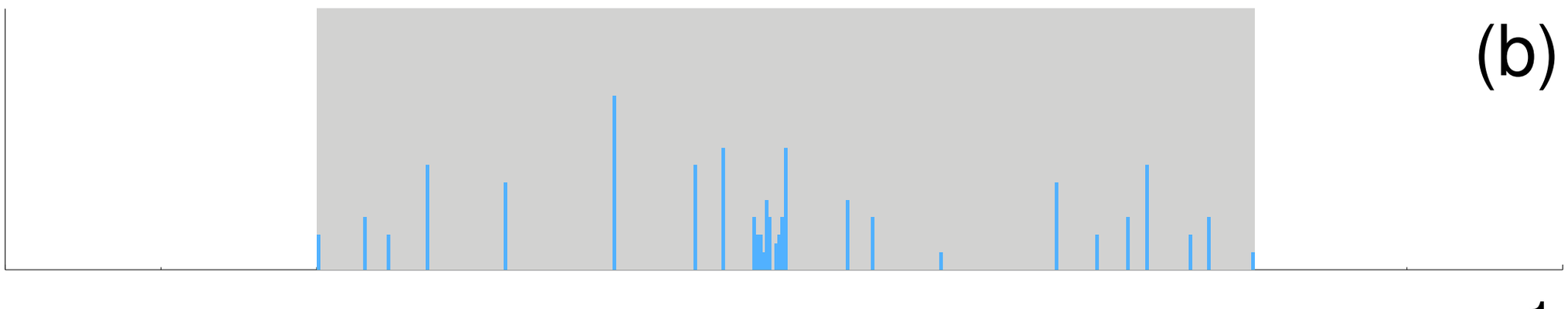

Series with Constituent Groups

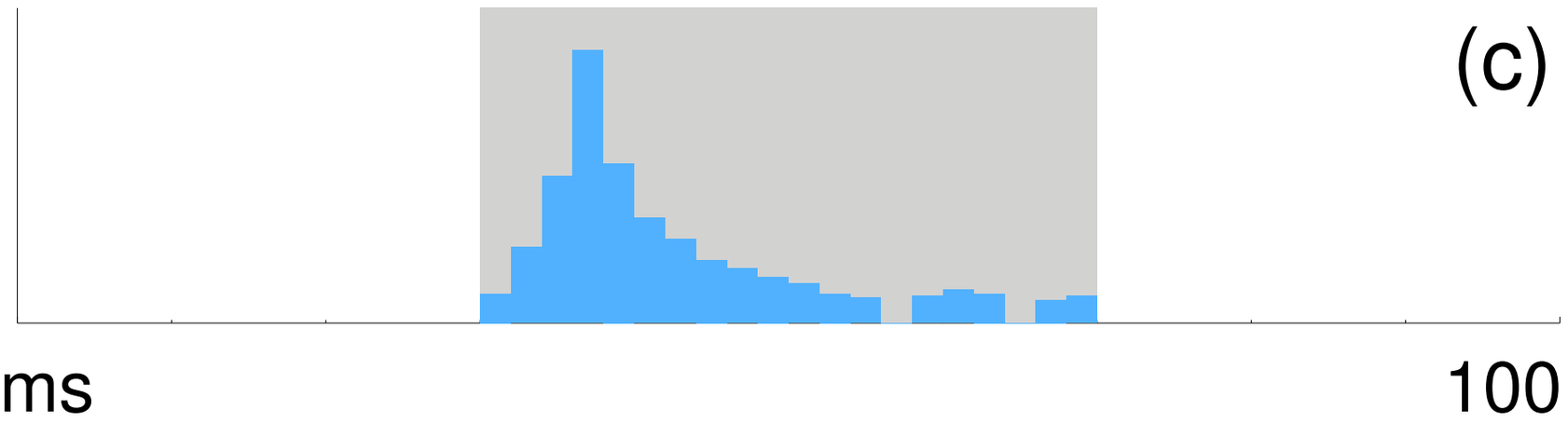

Event / Group with Constituent Samples

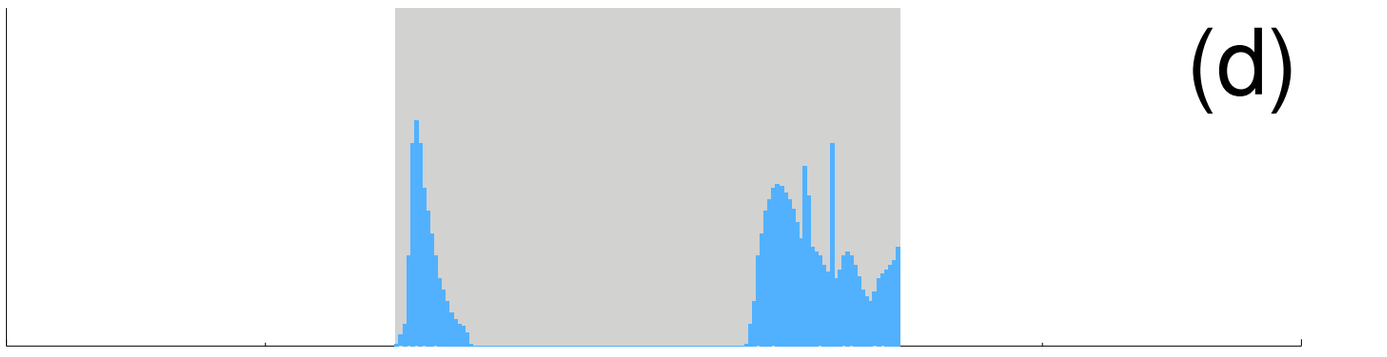

Pulse with Constituent Samples

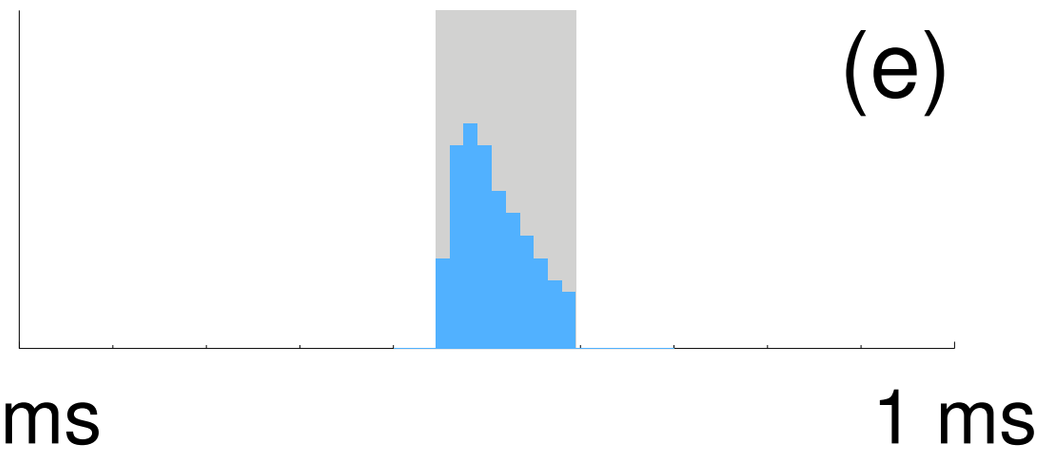

Sample

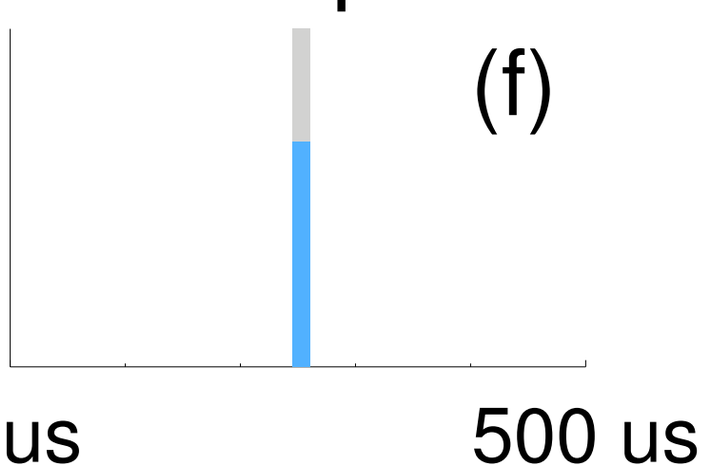

Figure 2.

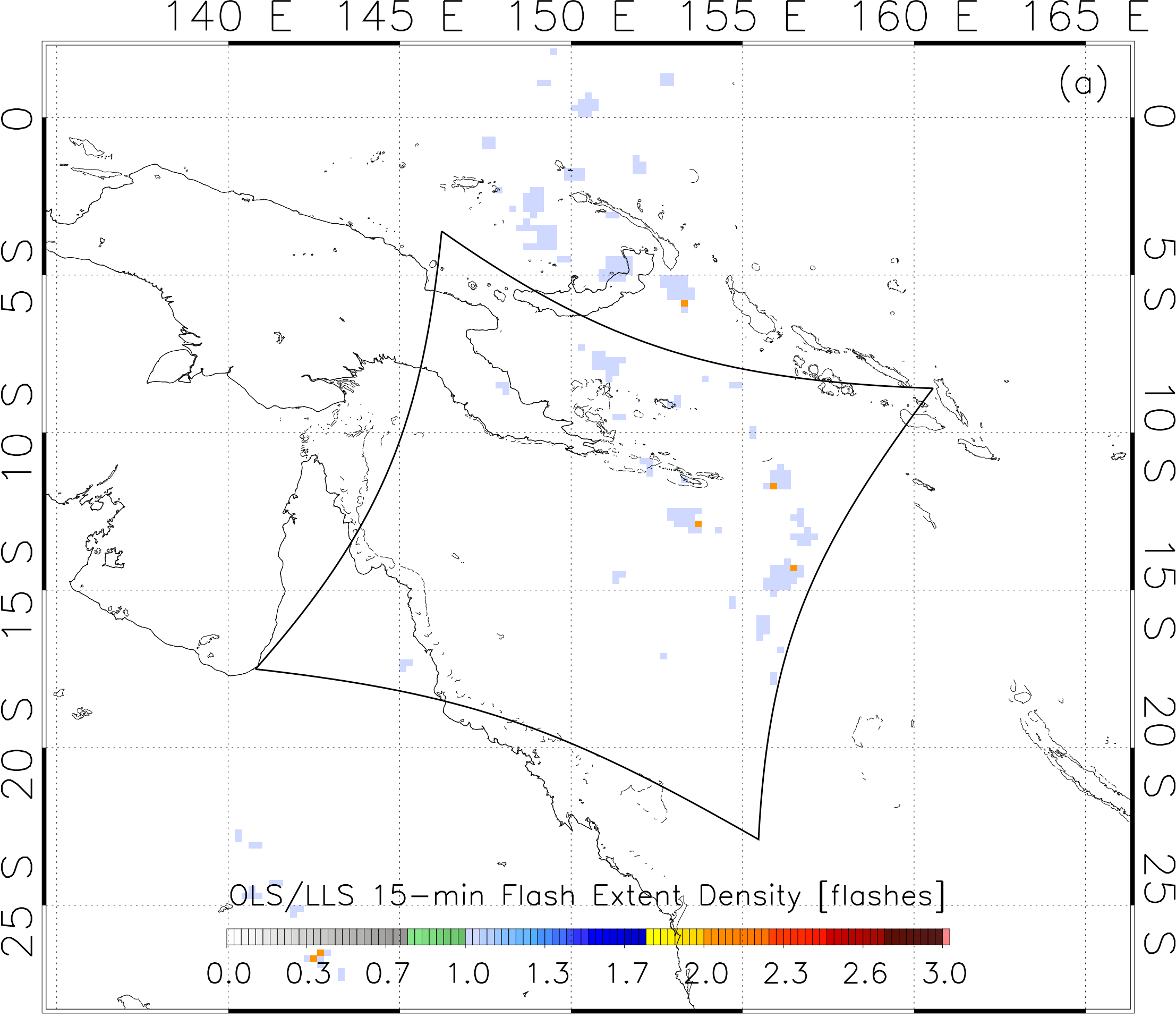
(a)
140 E
145 E
150 E
155 E
160 E
165 E
0
5 S
10 S
15 S
20 S
25 S
OLS/LLS 15-min Flash Extent Density [flashes]
0.0
0.3
0.7
1.0
1.3
1.7
2.0
2.3
2.6
3.0

(b)
RF
OLS / LLS
OLS / PDD
Trigger Count
0
10
20
30
40
50
60
−6
−4
−2
−60
−1
0
1
60
2
4
6
minutes
seconds
seconds
minutes
Time Since Flash First / Last Group

Figure 3.

Group Number

(a)

156.0 E

156.5 E

157.0 E

Group Energy [σ]

(b)

Freq. [%]

(c)

15.0 S

14.5 S

14.0 S

13.5 S

15.5 S

Percent of Total Flash Energy

0 1 3 4 6 8 9 11 13 14

(d)

155.5 S

155.0 S

154.5 S

154.0 S

153.5 S

0 5 10 15 20 25 30

Group Area [km^2]

(e)

Group Energy [σ]

(f)

Milliseconds since First Group

Figure 4.

OLS / LLS Group Energy

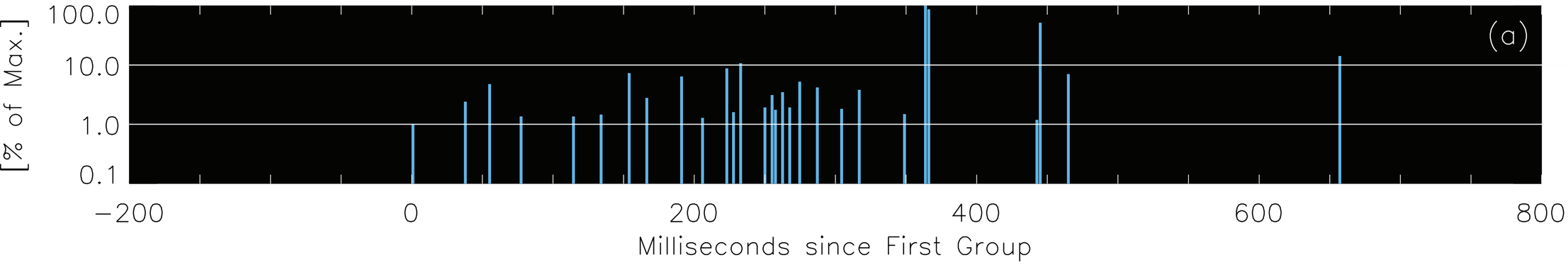

OLS / PDD Sample Energy

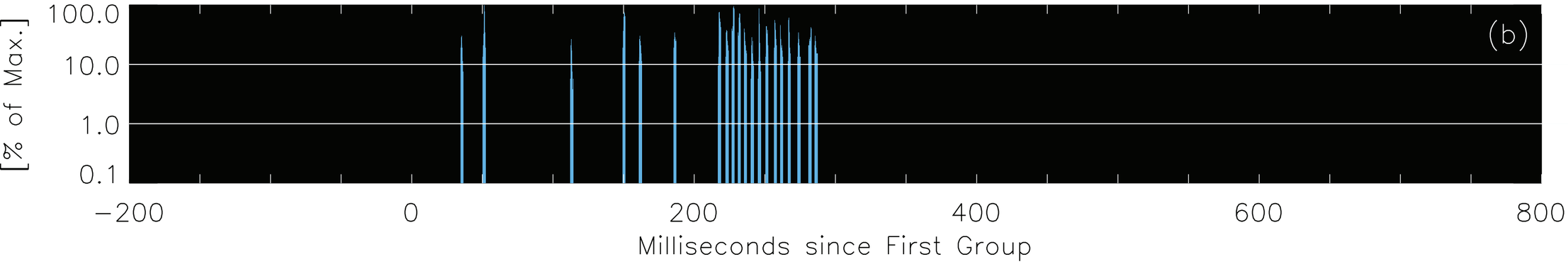

RF / TATRA Event Peak Power

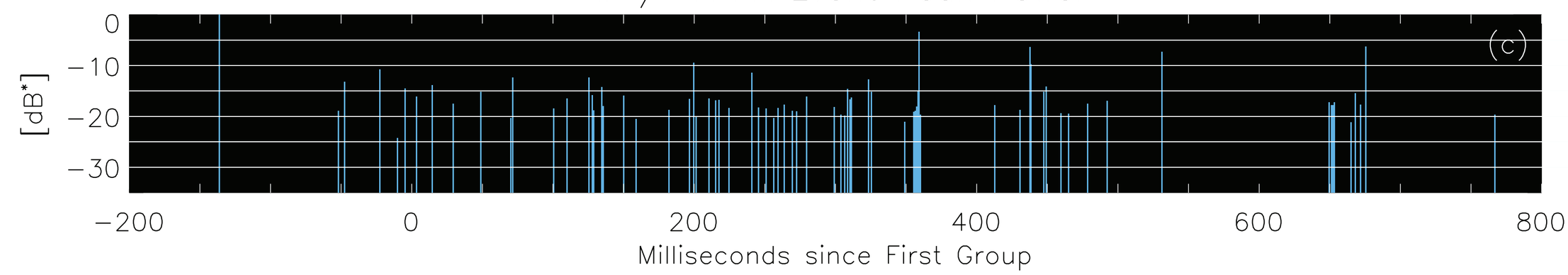

RF / TATRA Pulse Type Frequency (2−ms Window)

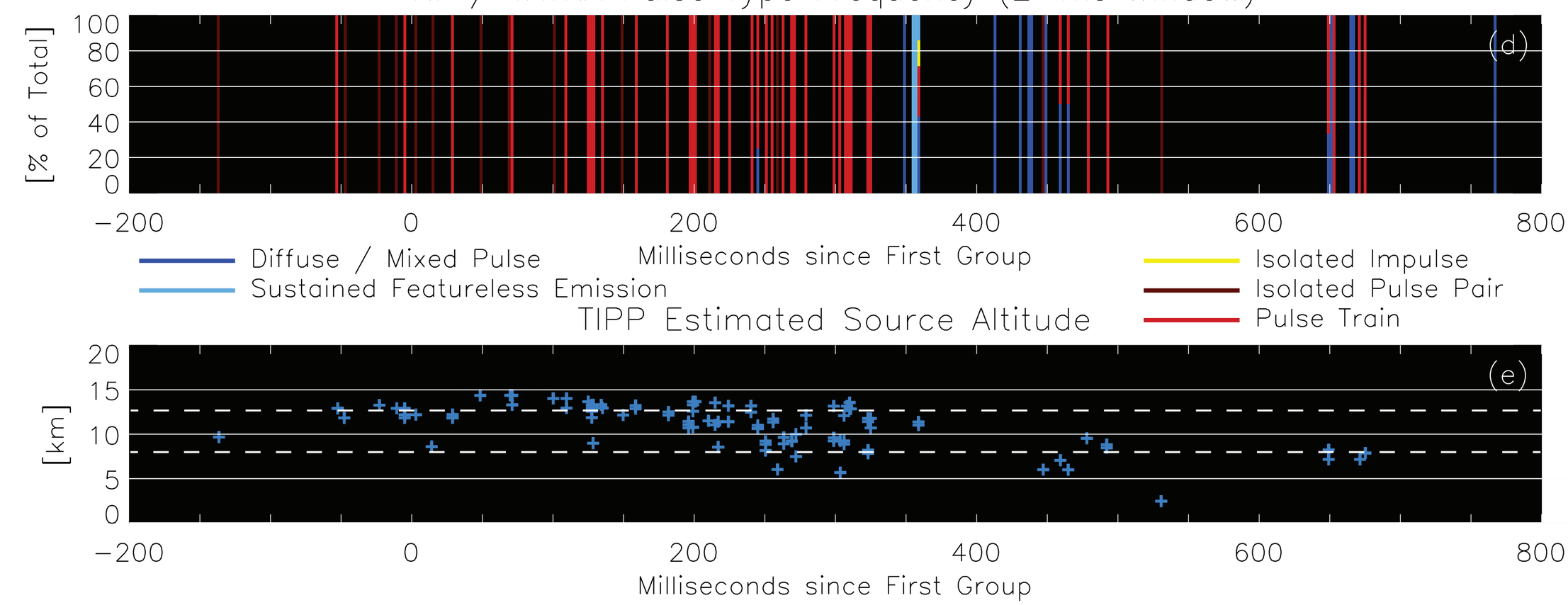

TIPP Estimated Source Altitude

Time−Integrated Received Optical and RF Energy

Figure 5.

Group Number

(a)

Group Energy [σ]

(b)

Freq. [%]

156.0 E

156.5 E

157.0 E

13.5 S

14.0 S

14.5 S

15.0 S

15.5 S

(c)

Percent of Total Flash Energy

0.0 0.6 1.1 1.7 2.2 2.8 3.3 3.9 4.4 5.0

(d)

OLS Energy [%]

(e)

RF Power [dB]

(f)

Milliseconds since First Group

Figure 6.

Group Number

Group Energy [σ]

(a)

(b)

Freq. [%]

(c)

(d)

Percent of Total Flash Energy

OLS Energy [%]

(e)

RF Power [dB]

(f)

Milliseconds since First Group

Figure 7.

(a)

Group Number

0
2
4

156.0 E
156.5 E
157.0 E

(b)

Group Energy [σ]

Freq. [%]

0
20
40
60
80
100

0
2
4

(c)

13.5 S
14.0 S
14.5 S
15.0 S
15.5 S

156.0 E
156.5 E
157.0 E

Percent of Total Flash Energy

0.0 0.6 1.1 1.7 2.2 2.8 3.3 3.9 4.4 5.0

(d)

13.5 S
14.0 S
14.5 S
15.0 S
15.5 S

0
2
4

(e)

OLS Energy [%]

100.0
10.0
1.0
0.1

354
356
358
360
362
364
366

(f)

RF Power [dB]

0
−10
−20
−30

Milliseconds since First Group

Figure 8.

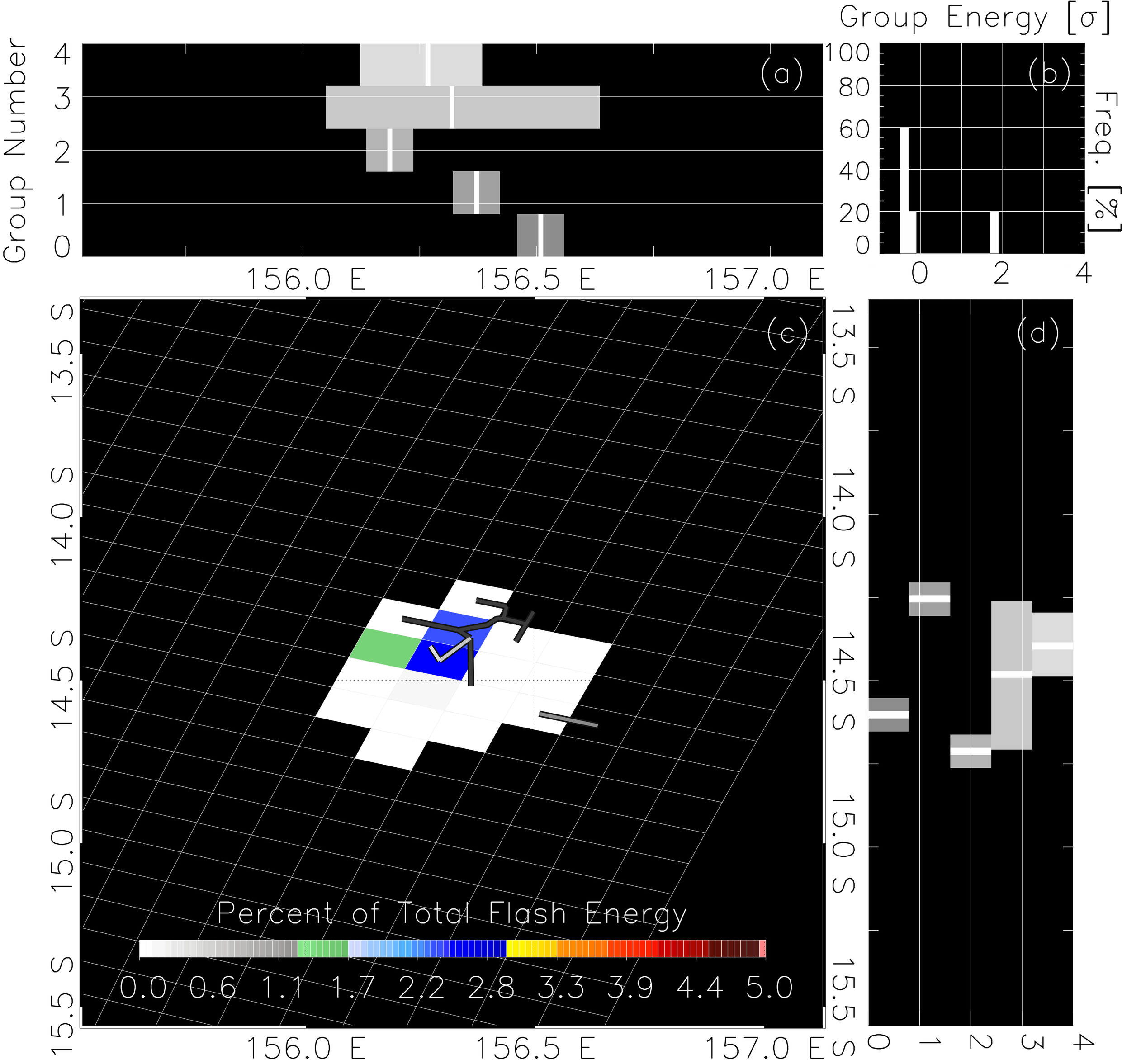
Group Energy [σ]
Group Number
(a)
(b)
Freq. [%]
156.0 E
156.5 E
157.0 E
13.5 S
14.0 S
14.5 S
15.0 S
15.5 S
(c)
(d)
Percent of Total Flash Energy
0.0 0.6 1.1 1.7 2.2 2.8 3.3 3.9 4.4 5.0

OLS Energy [%]
100.0
10.0
1.0
0.1
(e)
420
440
460
480
500
RF Power [dB]
0
−10
−20
−30
(f)
Milliseconds since First Group